

# Near-Infrared Spectral Monitoring of Triton with IRTF/SpeX II: Spatial Distribution and Evolution of Ices

W.M. Grundy<sup>1,2</sup>, L.A. Young<sup>1,3</sup>, J.A. Stansberry<sup>4</sup>, M.W. Buie<sup>3</sup>, and E.F. Young<sup>1,3</sup>

<sup>1</sup>Visiting/remote observer at the Infrared Telescope Facility, operated by the University of Hawaii under Cooperative Agreement NCC 5-538 with the National Aeronautics and Space Administration, Science Mission Directorate, Planetary Astronomy Program.

<sup>2</sup>Lowell Observatory, 1400 W. Mars Hill Rd., Flagstaff AZ 86001

<sup>3</sup>Southwest Research Institute, 1050 Walnut St., Boulder CO 80302

<sup>4</sup>Steward Observatory, Univ. of Arizona, 933 Cherry Ave., Tucson AZ 87721

— Submitted to *Icarus* 2009 May 11 —

Received \_\_\_\_\_; accepted \_\_\_\_\_

Primary contact: Will Grundy

E-mail: W.Grundy@lowell.edu

Voice: 928-233-3231

Fax: 928-774-6296

Running head: Distribution and evolution of Triton's ices

Manuscript pages: 51

Figures: 11

Tables: 5

## ABSTRACT

This report arises from an ongoing program to monitor Neptune’s largest moon Triton spectroscopically in the 0.8 to 2.4  $\mu\text{m}$  range using IRTF/Spex. Our objective is to search for changes on Triton’s surface as witnessed by changes in the infrared absorption bands of its surface ices  $\text{N}_2$ ,  $\text{CH}_4$ ,  $\text{H}_2\text{O}$ ,  $\text{CO}$ , and  $\text{CO}_2$ . We have recorded infrared spectra of Triton on 50 nights over the nine apparitions from 2000 through 2008. The data confirm our previously reported diurnal spectral variations of the ice absorption bands (Grundy and Young 2004). Nitrogen ice shows a large amplitude variation, with much stronger absorption on Triton’s Neptune-facing hemisphere. We present evidence for seasonal evolution of Triton’s  $\text{N}_2$  ice: the 2.15  $\mu\text{m}$  absorption band appears to be diminishing, especially on the Neptune-facing hemisphere. Although it is evidently dissolved in  $\text{N}_2$  ice, Triton’s  $\text{CH}_4$  ice shows a very different longitudinal variation from the  $\text{N}_2$  ice, challenging assumptions of how the two ices behave. Unlike Triton’s  $\text{CH}_4$  ice, the  $\text{CO}$  ice does exhibit longitudinal variation very similar to the  $\text{N}_2$  ice, implying that  $\text{CO}$  and  $\text{N}_2$  condense and sublimate together, maintaining a consistent mixing ratio.

*Subject headings:* Ices; Triton; Neptune, satellites; Infrared observations;  
Spectroscopy

## 1. Introduction

Despite its small size and frigid surface temperatures, Triton is a spectacularly dynamic world. Its geologically young surface (Croft *et al.* 1995; Stern and McKinnon 2000; Schenk and Zahnle 2007) is partially coated with a veneer of volatile ices which support and interact

with a seasonally-variable atmosphere. Having been imaged up-close by the Voyager II spacecraft in 1989, Triton’s role is crucial in guiding our thinking about surface-atmosphere interactions on as-yet-unexplored, small, icy planets like Pluto, Eris, and Makemake which have similar surface volatile inventories (e.g., Owen *et al.* 1993; Licandro *et al.* 2006; Tegler *et al.* 2008; Abernathy *et al.* 2009; Merlin *et al.* 2009). As reviewed by Grundy and Young (2004, hereafter “Paper 1”), Triton’s complex seasonal cycle is expected to drive large regional variations in solar heating, leading to dramatic changes in atmospheric pressure and seasonal redistribution of the volatile ices (e.g., Trafton *et al.* 1998). Observational evidence for ongoing seasonal change on Triton includes its evolving photometric colors at visible and ultraviolet wavelengths (Buratti *et al.* 1994; Young and Stern 2001) and its recently-expanding atmosphere (Elliot *et al.* 2000). There have also been tentative reports of short-term visible wavelength changes (Buratti *et al.* 1999; Hicks and Buratti 2004), as well as longer term evolution at near-infrared wavelengths (reviewed by Paper 1).

Reflectance spectroscopy in the near-infrared spectral region (0.7 to 2.5  $\mu\text{m}$ ) is especially sensitive to the composition, texture, and distribution of volatile ices on Triton’s surface. Observable changes at these wavelengths are expected as ices sublime or condense. We have been monitoring Triton’s near-infrared spectrum for nine years with a single instrument and telescope combination in an effort to detect spectral changes over a variety of timescales. These observations also yield information about the spatial distribution of Triton’s ices.

## 2. Observations and Reduction

We successfully observed Triton on 50 nights during 2000-2008 at NASA’s Infrared Telescope Facility (IRTF) on Mauna Kea, listed in Table 1. The data were collected using the short cross-dispersed mode of the SpeX spectrograph (Rayner *et al.* 1998, 2003), which

covers wavelengths from 0.8 to 2.4  $\mu\text{m}$ . From fall 2002 onward, most of the observations were done in brief 2 or 3 hour time allocations, taking advantage of the superior scheduling flexibility offered by the IRTF in conjunction with remote observing from the U.S. mainland (e.g., Bus *et al.* 2002).

EDITOR: Please place TABLE 1 near here.

Details of data acquisition and reduction strategies have been described previously (Paper 1; also Grundy *et al.* 2006). To remove telluric absorptions, instrumental effects, and the solar spectrum, all Triton observations were interspersed between observations of solar analog stars. During 2000-2001, we only used well known solar analogs 16 Cyg B, BS 5968, BS 6060, and SA 112-1333. Unfortunately, Neptune and Triton were far from these stars on the sky plane, resulting in slews large enough to give troublesome instrumental flexure between Triton and star observations. To remedy this, in 2002, we began using the much more nearby solar analog star HD 202282 (spectral class G3V, according to Houk and Smith-Moore 1988) after verifying with SpeX observations that its spectrum matched those of the better known analogs. Neptune’s heliocentric motion forced us to transition to a new nearby solar analog in 2008. We selected BS 8283, which, despite its being an unresolved G0V+G1IV binary system (Neckel 1986; Pourbaix *et al.* 2004), has proven to be spectrally similar enough to the Sun for our purposes.

Wavelength calibration was derived from telluric sky emission lines extracted from the Triton frames. Profiles of these lines during 2002-2008 (when we used SpeX’s 0.3 arcsec slit, in order to maintain as consistent as possible spectral resolution) resembled Gaussians having full width at half maximum ( $FWHM$ ) of  $\sim 2.5$  pixels, implying spectral resolution ( $\lambda/FWHM$ ) between 1600 and 1700. Prior to 2002 we used a wider slit (0.5 arcsec) to admit more light, resulting in measured spectral resolutions in the 1300 to 1400 range.

Wavelength uncertainty is less than a pixel in regions having abundant night sky lines. The spectra were not photometrically calibrated, due to variable slit losses from distinct tracking and guiding correction timescales between bright calibration stars and much fainter Triton, along with variable focus and seeing conditions. Also, many of our spectra were collected on non-photometric nights. An average spectrum appears in Fig. 1; examples of individual nightly spectra were shown in Paper 1.

EDITOR: Please place FIGURE 1 near here. For the convenience of reviewers, figure callouts are hereafter indicated by a thumbnail of the figure, plus its caption.

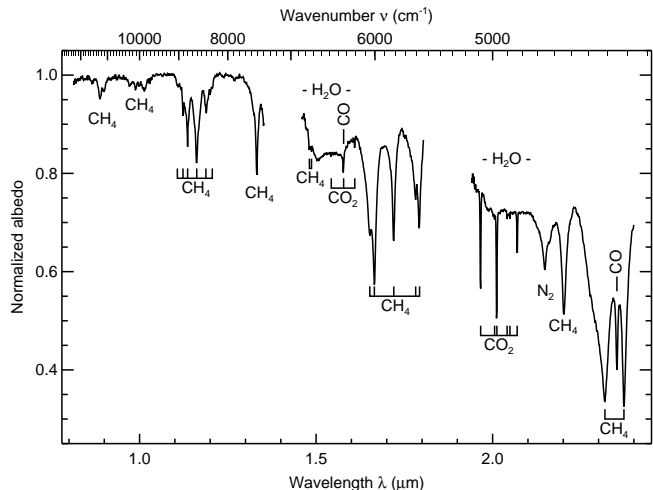


**Fig. 1:** Average IRTF/SpEx spectrum of Triton. Vibrational absorptions by various ice species are labeled. These are generally overtones and combinations of longer wavelength fundamental modes. Gaps around 1.4 and 1.9  $\mu\text{m}$  coincide with higher opacity in the terrestrial atmosphere.

### 3. Longitudinal Distributions of Ice Species

Based on eight nights of data obtained in 2002, Paper 1 reported diverse patterns of longitudinal variability for Triton’s different ice species. The strongest variation, by almost a factor of two, was seen in the 2.15  $\mu\text{m}$   $\text{N}_2$  ice absorption band, implying a very uneven regional distribution of that species, heavily biased toward low latitudes and the Neptune-facing hemisphere. Regional variations in  $\text{N}_2$  ice texture could also explain the observed variation, by causing longer mean optical path lengths in those regions. The

CH<sub>4</sub> ice bands were seen to vary less, and to exhibit maximum absorption at longitudes shifted toward the trailing hemisphere. This observation was puzzling in light of the fact that Triton’s CH<sub>4</sub> ice is dissolved in N<sub>2</sub> ice (Quirico *et al.* 1999). Triton’s water ice absorption was reported to be slightly stronger on the leading hemisphere, while little if any longitudinal variation was seen in the CO<sub>2</sub> ice bands, implying a globally homogeneous or high latitude distribution of that species. Now, with our much larger set of spectra from 50 separate nights, we can test the validity of the longitudinal patterns reported earlier as well as searching for additional, more subtle trends not detected in the previous, sparser data set.

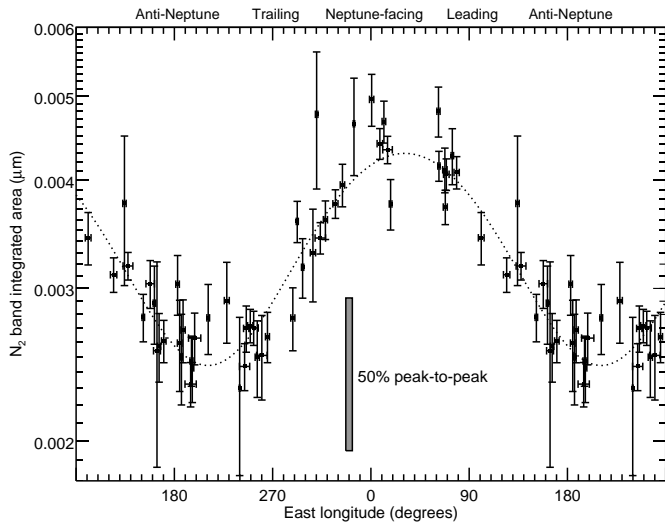


**Fig. 2:** Integrated area of the 2.15  $\mu\text{m}$  N<sub>2</sub> ice absorption band as a function of sub-Earth longitude on Triton, showing a large periodic variation as Triton rotates. A logarithmic scale is used to facilitate comparison with similar plots to be shown for other ice species. Each point represents observations from a single night, with points duplicated over an additional 180° to better show the cyclic pattern. The dotted curve is a sinusoid fitted to the data.

The large amplitude longitudinal variation in Triton’s N<sub>2</sub> ice reported in Paper 1 is confirmed by the new data, as shown in Fig. 2. A sinusoid fitted to the integrated absorption data has its maximum at  $31 \pm 3^\circ$  East sub-Earth longitude and a peak-to-peak amplitude of  $76 \pm 4$  percent (comparable to, but smaller than the  $96 \pm 16$  percent variation reported in Paper 1). We measure integrated absorption by normalizing each spectrum

to a line fitted to continuum wavelengths on either side of the absorption band (2.093 to 2.117  $\mu\text{m}$  and 2.175 to 1.185  $\mu\text{m}$ , in the case of this  $\text{N}_2$  ice band), then integrating one minus the normalized spectrum over the band interval (2.117 to 2.175  $\mu\text{m}$ , for this band). We also note that the width and shape of Triton’s  $\text{N}_2$  band are consistent with the hexagonal  $\beta$  phase of  $\text{N}_2$  ice which is stable above 35.6 K, and not the lower temperature, cubic,  $\alpha$  phase (Scott 1976). Additionally, the presence of the shoulder at about 2.16  $\mu\text{m}$  indicates that the temperature of the  $\text{N}_2$  ice is below about 41 K (Paper 1; Grundy *et al.* 1993; Tryka *et al.* 1993).

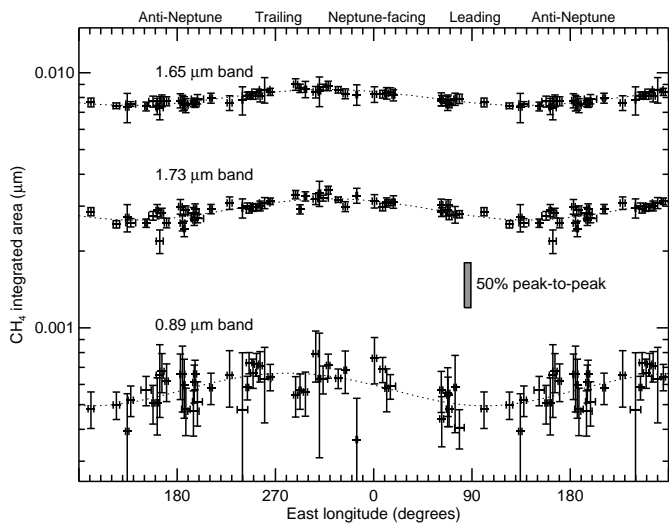


**Fig. 3:** Integrated areas of three  $\text{CH}_4$  ice absorption bands as a function of sub-Earth longitude on Triton, showing periodic variations as Triton rotates. Other features are as described in Fig. 2.

Triton’s methane ice produces numerous absorption bands, which combine to form a series of band complexes diminishing in strength toward shorter wavelengths (see Fig. 1). Paper 1 reported longitudinal variations for three  $\text{CH}_4$  bands, at 0.89, 1.65, and 1.73  $\mu\text{m}$ , showing maximum absorption on the trailing hemisphere. The new data confirm the earlier results for those three bands (see Fig. 3) and also show similar behavior for the 1.15, 1.33, and 2.2  $\mu\text{m}$   $\text{CH}_4$  ice bands (which are omitted from Fig. 3 to reduce clutter). Wavelengths used in computing integrated absorptions throughout this paper are listed in Table 2. From sinusoids fitted to the integrated absorptions, maximum absorption for the six  $\text{CH}_4$  bands are all near  $300^\circ$  East longitude, corresponding to the Neptune-facing part of the trailing

hemisphere. Parameters of these fits are listed in Table 3. Since Triton’s  $\text{CH}_4$  is dissolved in  $\text{N}_2$  ice (Quirico *et al.* 1999), one might expect the two ices to share the same longitudinal distribution. Clearly, the new data confirm that not to be the case. Triton’s  $\text{CH}_4$  and  $\text{N}_2$  ices evidently do not simply co-occur with a constant mixing ratio. Their mixing ratio must be a function of longitude. Additional clues to the nature of this regionally variable dilution can also be gleaned from the wavelengths of the  $\text{CH}_4$  absorptions, to be described later.

EDITOR: Please place TABLE 2 near here.

EDITOR: Please place TABLE 3 near here.

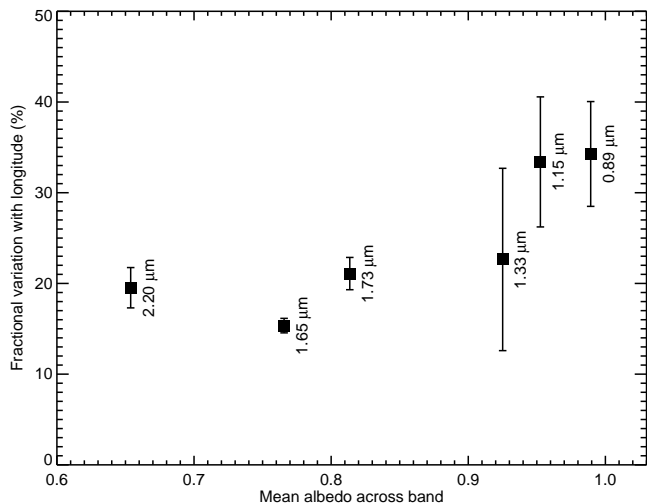


**Fig. 4:** Fractional longitudinal variation of six  $\text{CH}_4$  ice absorption bands (labeled according to their wavelengths) as a function of average albedo across the band. In general, weaker bands with higher average albedos sample deeper within the surface. These weaker bands show greater longitudinal variation. The  $1.65 \mu\text{m}$   $\text{CH}_4$  band coincides with a water ice band, which may reduce its apparent variability, since  $\text{H}_2\text{O}$  absorption is stronger on the leading hemisphere, as will be discussed shortly.

Triton’s shallower, shorter-wavelength  $\text{CH}_4$  bands at  $0.89$  and  $1.15 \mu\text{m}$  exhibit stronger fractional variation with longitude ( $34 \pm 6\%$  and  $33 \pm 7\%$  peak-to-peak, respectively) than the deeper, longer-wavelength bands at  $1.65$ ,  $1.73$ , and  $2.2 \mu\text{m}$  ( $15 \pm 1\%$ ,  $21 \pm 2\%$ , and

$20\pm 2\%$ , respectively), as shown in Fig. 4. In general, weaker absorption bands sample more deeply within a surface than their counterparts at more strongly absorbing wavelengths (e.g., Grundy and Fink 1996; Tegler *et al.* 2008; Abernathy *et al.* 2009; Merlin *et al.* 2009). A trend of greater longitudinal variation for shallower bands suggests that regions with thicker deposits and/or higher concentrations of  $\text{CH}_4$  ice capable of producing appreciable absorption in the weaker bands are more heterogeneously distributed than the relatively shallow and/or highly-diluted layer of  $\text{CH}_4$ -containing ice responsible for the stronger  $\text{CH}_4$  absorptions. Perhaps most of the observed longitudinal variation in Triton’s  $\text{CH}_4$  bands comes from relatively isolated, low-latitude regions of deep or  $\text{CH}_4$ -rich ice. These regions would need to be preferentially located on the trailing hemisphere, unlike the  $\text{N}_2$  ice which shows more absorption on the leading part of the sub-Neptune hemisphere.

Our data confirm that Triton’s  $\text{CH}_4$  bands are blue-shifted relative to the wavelengths of pure  $\text{CH}_4$  ice absorption bands, indicating that Triton’s  $\text{CH}_4$  is diluted in  $\text{N}_2$  ice (e.g., Quirico and Schmitt 1997; Quirico *et al.* 1999; Grundy *et al.* 2002a). Blue shifts relative to the shifts reported for highly-diluted  $\text{CH}_4$  by Quirico and Schmitt (1997) are shown as a function of sub-observer longitude in Fig. 5, as measured by autocorrelation. A sinusoidal fit to these measurements shows shifts ranging from 89% to 100% of that expected for  $\text{N}_2$ -isolated  $\text{CH}_4$ . The peak-to-peak variation of this sinusoid is  $0.111\pm 0.010$  in these units, an  $\sim 11\text{-}\sigma$  detection of longitudinal variation. The least diluted  $\text{CH}_4$  appears on trailing-hemisphere longitudes where  $\text{CH}_4$  absorption bands are strongest, implying that higher  $\text{CH}_4$  concentration in  $\text{N}_2$  is at least partially responsible for enhancing  $\text{CH}_4$  absorption at those longitudes.

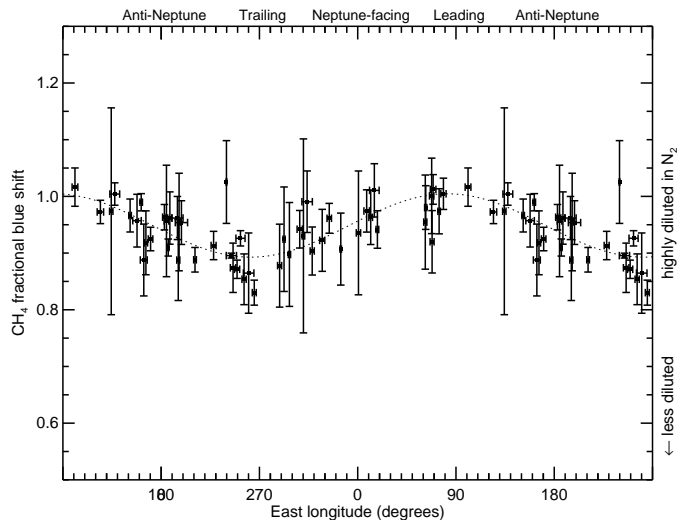


**Fig. 5:** Average blue shift of Triton’s 1.65, 1.73, and 2.2  $\mu\text{m}$   $\text{CH}_4$  ice absorption bands, relative to the shifts reported by Quirico and Schmitt (1997) for  $\text{CH}_4$  molecules isolated in  $\text{N}_2$  ice. In this plot, a value of zero would correspond to pure  $\text{CH}_4$  ice while a value of one indicates ice in which each  $\text{CH}_4$  molecule has exclusively  $\text{N}_2$  molecules for neighbors. However, a value of 0.9 should not be interpreted as necessarily implying a 90%  $\text{N}_2$  and 10%  $\text{CH}_4$  composition, since the dependence of the shift on concentration is not yet well understood (Cornelison *et al.* 2008; Brunetto *et al.* 2008).  $\text{CH}_4$  is not even soluble in  $\text{N}_2$  ice at 10% concentration, so at least two distinct phases would have to be present at that composition (Prokhvatilov and Yantsevich 1983; Lunine and Stephenson 1985).

The longitudinal variation of Triton’s  $\text{H}_2\text{O}$  ice is trickier to quantify. Although the distinctive shapes of crystalline  $\text{H}_2\text{O}$  ice bands at 1.55 and 2  $\mu\text{m}$  are obvious in the spectra (see Fig. 1 and discussion in Paper 1), these bands are so broad that they straddle gaps in wavelength coverage as well as overlapping other absorption bands, preventing numerical integration of their areas. Still, it is possible to construct albedo ratios which are sensitive to  $\text{H}_2\text{O}$  ice absorption. One minus the mean albedo between 1.505 and 1.57  $\mu\text{m}$  divided

by the mean albedo between 1.25 and 1.27  $\mu\text{m}$  and between 1.73 and 1.75  $\mu\text{m}$  crudely measures the fractional band depth of the 1.5  $\mu\text{m}$  H<sub>2</sub>O ice band complex. This quantity is shown in Fig. 6. This plot shows a similar trend to what was reported in Paper 1, with an enhancement by  $12\pm 3\%$  (peak-to-peak in a sinusoidal fit) in H<sub>2</sub>O ice absorption on Triton’s leading hemisphere. A similar pattern of deeper H<sub>2</sub>O ice absorption bands on leading hemispheres has been seen on many icy satellites of Jupiter, Saturn, and Uranus (Grundy *et al.* 1999, 2006). This tendency may be related to higher rates of impact cratering and higher impact velocities on leading hemispheres (Zahnle *et al.* 2001, 2003).

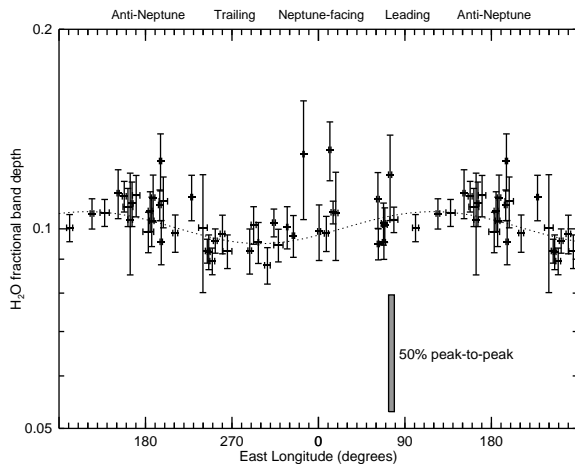


**Fig. 6:** Fractional band depth of H<sub>2</sub>O ice as a function of sub-Earth longitude on Triton, showing a subtle enhancement of H<sub>2</sub>O ice absorption on the leading hemisphere ( $12\pm 3\%$  peak-to-peak from the sinusoidal fit shown as a dotted curve).

In Paper 1 we reported no measurable longitudinal variation of Triton’s CO<sub>2</sub> absorption bands around 2  $\mu\text{m}$ . The new data confirm that result, as shown in Fig. 7. To produce such remarkably little variation as Triton rotates, the CO<sub>2</sub> ice must be very uniformly distributed and/or be confined to high southern latitudes. Being completely non-volatile at Triton surface temperatures, one might expect Triton’s CO<sub>2</sub> ice to be distributed similarly to the non-volatile H<sub>2</sub>O ice, but these data show subtle but apparently significant differences between the longitudinal distributions of these two inert ices.

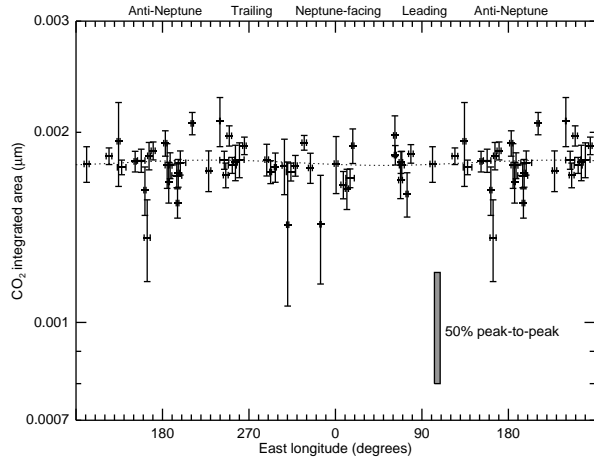


**Fig. 7:** Total integrated area of three narrow CO<sub>2</sub> ice absorption bands near 2 μm as a function of sub-Earth longitude on Triton, showing no significant evidence of longitudinal variability ( $2\pm 2\%$  peak-to-peak from the sinusoidal fit shown as a dotted curve).

Finally, we turn to carbon monoxide ice. CO has two narrow absorption bands in our wavelength region. The 0-3 overtone at 1.578 μm coincides with a narrow CO<sub>2</sub> band and with the corner of a square-bottomed crystalline H<sub>2</sub>O ice band, making it effectively unmeasurable. The stronger, 0-2 overtone at 2.352 μm falls between two particularly deep CH<sub>4</sub> absorption bands (see Fig. 1). We can compute an integrated area for this band using 2.343 to 2.356 μm for the band and 2.338 to 2.343 μm and 2.356 to 2.362 μm for the continuum, as shown in Fig. 8. The resulting area is likely to be somewhat contaminated by CH<sub>4</sub> absorption in the continuum wavelengths, but as the measured longitudinal variation is much stronger than seen for CH<sub>4</sub> absorptions (especially the stronger CH<sub>4</sub> bands), we believe this pattern is mostly due to actual variation in CO absorption. A sinusoidal fit gives a peak-to-peak variation of  $71\pm 7\%$  with the maximum on the leading side of the sub-Neptune hemisphere. This distribution looks very similar to what was seen for N<sub>2</sub> absorption (see Fig. 2), suggesting that, unlike CH<sub>4</sub> ice, CO ice is globally accompanied by N<sub>2</sub> ice. We note that the volatilities of CO and N<sub>2</sub> ices are very similar to one another, while CH<sub>4</sub> ice is much less volatile (Brown and Ziegler 1980). However, we note that the peaks of the sinusoidal fits to the N<sub>2</sub> and CO absorption variations seem to be shifted from one another, by amounts that seem to be statistically significant ( $31\pm 3$  and  $58\pm 5$  for N<sub>2</sub> and CO, respectively). That the CO absorption should be shifted slightly relative to the N<sub>2</sub>

absorption is puzzling.

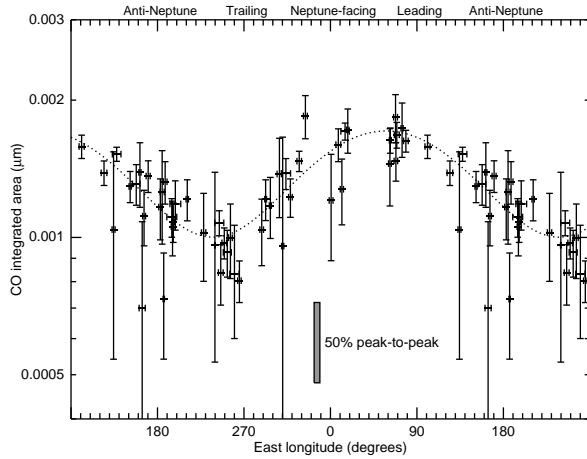


**Fig. 8:** Integrated area of the narrow CO ice absorption band at  $2.352 \mu\text{m}$  as a function of sub-Earth longitude on Triton, showing a very similar pattern to that of  $\text{N}_2$  ice.

To summarize the observed longitudinal variations, we compare in Fig. 9 the different patterns of variation seen for absorption bands of the five ice species as Triton rotates about its axis. The  $\text{N}_2$  and CO absorptions show the greatest magnitude of variation, and their variations appear quite similar to one another, implying similar geographic distributions. The absorption variations for various methane bands are similar to one another, so this plot shows only two representative examples: a strongly absorbing band at  $1.73 \mu\text{m}$  and a weakly absorbing one at  $0.89 \mu\text{m}$ .  $\text{H}_2\text{O}$  and  $\text{CO}_2$  ice absorptions show comparatively little variation as Triton rotates.

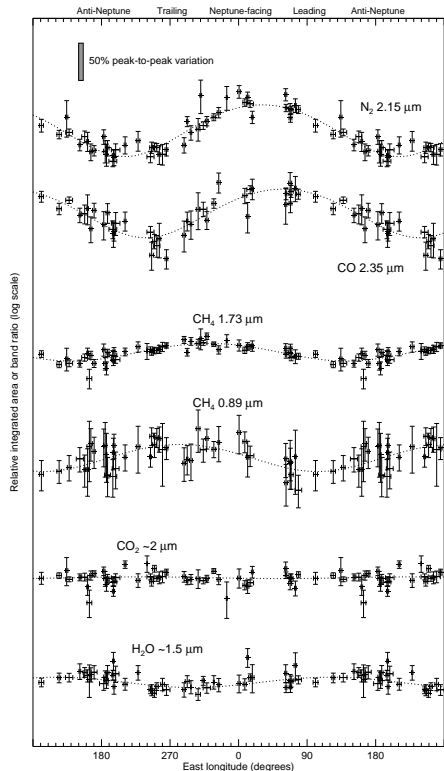


**Fig. 9:** Triton’s observed longitudinal spectral variations shown on a consistent logarithmic scale of relative variation.

#### 4. Search for Secular Change

Triton has been experiencing a major southern summer in recent decades, with the sub-Solar latitude reaching a maximum of  $50^\circ$  South latitude during the years 2000-2001. Since then, the sub-Solar latitude has begun slowly moving back toward the equator (see Table 1, noting that sub-Earth and sub-Solar points differ by the phase angle). Continuous sunlight falling on  $N_2$  ice at high southern latitudes should cause the ice to sublimate at rates of the order of centimeters per Earth year (e.g., Trafton *et al.* 1998).

To search for evidence of ice recession, we split our data into two groups, 24 nights of data collected during 2000-2004.5 and 26 nights collected during 2004.5-2009. Separate sinusoidal fits to the two groups are shown in Fig. 10. The most notable difference is that the later data show less scatter than the earlier data, having benefited from more consistent and polished acquisition techniques, as well as a number of measures taken by IRTF staff which considerably improved the telescope’s image quality. The earlier data generally fall above the dashed curve fitted to the entire data set, especially around the higher parts of that curve near zero longitude (Triton’s Neptune-facing hemisphere). The maxima of the two sinusoidal fits to the data subsets are  $4.46 \pm 0.08$  nm and  $4.18 \pm 0.07$  nm for 2000-2004.5 and 2004.5-2009, respectively, amounting to an apparently significant direct detection of changes in  $N_2$  ice distribution due to seasonal volatile transport on Triton. However, this evidence for seasonal loss of  $N_2$  ice from Triton’s summer hemisphere clearly needs testing with additional observations. Its verification will be complicated by the change of Triton’s sub-Solar latitude, which will be moving toward the equator at an accelerating pace over the coming years. That changing geometry will add an additional source of secular spectral changes which may be difficult to disentangle from changes caused by volatile transport.

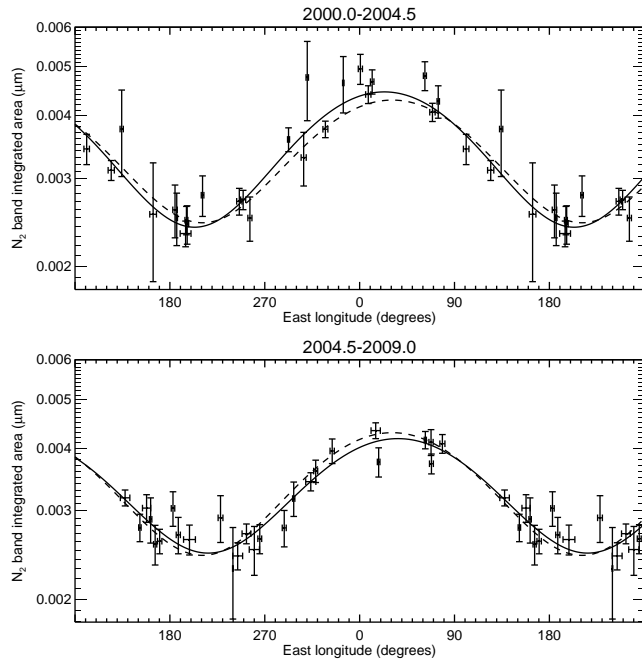


**Fig. 10:** Integrated area of the  $2.15 \mu\text{m}$   $\text{N}_2$  ice absorption band split into two 4.5-year time periods. In both panels, the solid curve is a sinusoidal fit to just the data taken during that interval, while the dashed curve is a fit to the full 9-year data set (also shown in Figs. 2 and 9).

We have seen no convincing evidence for transient changes in our spectra, such as have been reported at visible wavelengths (Buratti *et al.* 1999; Hicks and Buratti 2004). Outlier points do appear in our plots, but they are not more abundant than would be expected from our error statistics. Additionally, the outliers tend to correspond to nights with poor sky conditions or when something went wrong (equipment, software, power, or network failure, or observer error) which prevented us from collecting as much Triton or solar analog data as we had intended.

## 5. Discussion

Here we explore what the observed longitudinal patterns and secular evolution of Triton’s ices can tell us about their spatial distributions and temporal behaviors. We begin with the volatile ices  $\text{N}_2$  and  $\text{CO}$ , which are expected to migrate around Triton’s surface on seasonal timescales. Previous investigators constructed suites of longitudinally averaged models for ranges of unknowns such as the thermal inertia, emissivity, and the inventory

of  $N_2$ , and compared these with Voyager-era data, such as albedo and color maps and the atmospheric pressure (e.g., Hansen and Paige 1992; Spencer and Moore 1992). This work was hampered by the fact that Voyager’s instruments could not distinguish between Triton’s ice species. We take a different approach, beginning with our observations of spectral variations as Triton rotates and combining them with other constraints in an attempt to learn where those ices are presently located and thus advance our understanding of Triton’s seasonal cycles and surface-atmosphere interaction. Although the observed spectral variations could conceivably be caused by a wide variety of mechanisms, such as longitudinal variations in texture or stratigraphy, we start with the simpler hypothesis that they reflect the projected area of geological units composed of the different ices.

In Paper 1, we considered various combinations of the six McEwen (1990) color units as possible locations of Triton’s  $N_2$  ice. We found that no combination of these units had the same rotational variation as the  $N_2$  band depth. However, if the  $N_2$  were confined to portions of those units North of  $\sim 31^\circ$  South latitude, combinations could be found which produced patterns of  $N_2$  variation like those observed. To be more quantitative, for each combination of the McEwen units (plus the region unmapped by Voyager II, which we are calling Unit 0) we found the best-fitting cut-off latitude and  $N_2$  band integrated area in the  $N_2$  absorption-producing region. Combinations having low  $\chi^2_\nu$  values are listed in Table 4.

EDITOR: Please place TABLE 4 near here.

We also tried an alternative approach, based on a simple thermal balance model. From the bolometric hemispherical albedo map of Triton (i.e., the spatially resolved analog of the bolometric bond albedo; Stansberry *et al.* 1992) we calculated a map of diurnal average Solar energy absorption as Triton rotates. We reasoned that areas of Triton’s surface above some average energy absorption threshold should experience net sublimation of nitrogen

ice, the loss of which is balanced by net condensation in regions receiving less energy. We additionally assumed that an equilibrium is rapidly reached in which regions receiving more than the threshold energy are denuded of  $N_2$  ice while regions below that threshold are covered with it. Alternatively, we could assume that  $N_2$  ice remains present in regions experiencing net sublimation but that its texture evolves in such a way that little or no  $2.15 \mu\text{m}$  absorption is seen, whereas condensing regions rapidly acquire a texture which produces an observable absorption band. Regardless, we make the energy threshold and the integrated area of the  $N_2$  absorption band in  $2.15 \mu\text{m}$  absorbing areas free parameters and find the values which give the best fit to the observations. The goodness of fit for this model is  $\chi^2_\nu = 1.33$ , for a diurnal average energy threshold of  $79.7 \text{ erg cm}^{-2} \text{ s}^{-1}$  and a  $2.15 \mu\text{m}$   $N_2$  band integrated area of  $0.012 \mu\text{m}$ .

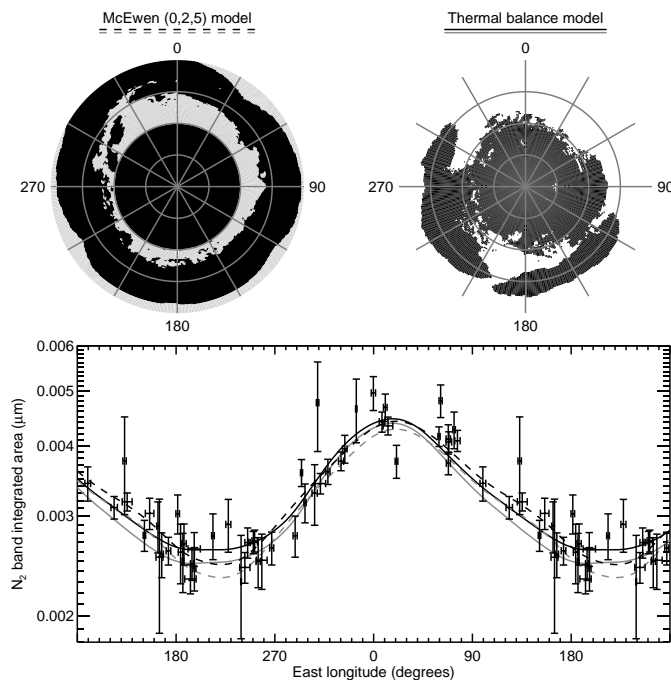


**Fig. 11:** Two models for the spatial distribution of Triton’s  $N_2$  ice in South polar projection, with areas free of  $N_2$  ice shown in black and areas covered with  $N_2$  shown in white. Longitude and latitude lines are at  $30^\circ$  intervals. The bottom panel shows the longitudinal variation in the  $N_2$  integrated area, as in Fig. 2. The black curves show the behavior of the McEwen units model (dashed) and the thermal balance model (solid). Gray versions of these curves show how the two models might respond to seasonal recession of  $N_2$  ice coverage.

Both of these very different approaches give reasonable matches to the observations, albeit with dissimilar spatial distributions, as shown in Fig. 11. Neither is formally excluded by the data. One could also imagine other models giving comparably good fits. So we conclude that the longitudinal variability plus a model such as one of these is not going to give us a unique map of where Triton’s  $N_2$  absorption occurs. However, both approaches do call for high Southern latitudes not to contribute to the observed  $2.15 \mu\text{m}$  absorption.

These models call for  $N_2$  band integrated areas for  $N_2$ -covered regions in the range of  $0.012\text{-}0.021 \mu\text{m}$ . Are such band areas even plausible for  $N_2$  ice? An integrated absorption of  $0.02 \mu\text{m}$  in  $N_2$  ice at 38 K (optical constants from Grundy *et al.* 1993) requires a mean optical path length within  $N_2$  ice of about a meter. Such a path length would be produced by a 43 cm thick slab of  $N_2$  ice above a scattering substrate, when viewed at a mean angle of  $30^\circ$  from the zenith, or by a particulate surface consisting of irregular, but smooth-surfaced  $\sim 7$  cm  $N_2$  ice “grains” (using ray-tracing procedures described by Abernathy *et al.* 2009). Both of these scenarios describe rather unusual surface textures. But such extreme textures seem to be required to provide the mean optical path lengths called for by the observational data, if Triton’s  $N_2$  absorption band is produced in only a fraction of the total projected surface area, as implied by the observed longitudinal variation.

One possible way to differentiate between  $N_2$  ice distribution models such as these is to consider their responses to seasonal recession of  $N_2$  ice, in comparison with the secular trends shown in Fig. 10. For the McEwen units model, we simulated seasonal recession by shifting the cut-off latitude Northward slightly, and for the thermal balance model, we did it by decreasing the cut-off energy slightly. The integrated area in  $N_2$ -covered areas was held constant. Both simulations resulted in slightly weaker  $N_2$  absorption because less area was covered by  $N_2$  ice, as shown with gray curves in Fig. 11). The greatest diminution was at longitudes where the  $N_2$  absorption was already weakest, leading to increasing fractional

variation. This evolutionary pattern differs from that described in Section 4 and shown in Fig. 10. If instead of changing N<sub>2</sub> ice areal coverage, seasonal evolution changes the texture of the ice in a way which reduces the band integrated area, N<sub>2</sub> absorption would drop most at the longitudes where the most N<sub>2</sub> absorption is seen, more consistent with Fig. 10. Textural evolution of the N<sub>2</sub> ice is expected from the solar gardening mechanisms described by Grundy and Stansberry (2000), although it is not clear that the trend should be toward the shorter mean optical path lengths in N<sub>2</sub> ice necessary to produce a diminishing absorption band.

A completely different approach involves considering the depths of the observed absorption bands. Imagine a region covered with a material that absorbs some fraction of the light from an absorption band, relative to reflectance at a continuum wavelength, surrounded by a region which reflects the same at both wavelengths. The most that the absorbing region can absorb is 100% of the light in the absorption band, so if, in a disk integrated spectrum, that band is 10% deep relative to continuum wavelengths, at least 10% of the observable projected area of the body must have that absorbing material present. This number is a very crude lower limit, since a much larger area could be covered if the absorption in the region in question was less than 100%. The shapes of Triton’s absorption bands are consistent with being shallower than 100%, since 100% saturated bands tend to appear broadened, with flat bottoms. A smaller area could be covered if the uncovered area had unrelated absorption at the same wavelength, such as for CO<sub>2</sub> and H<sub>2</sub>O, both of which absorb at 2.01  $\mu\text{m}$ . This situation creates ambiguities in assessing the appropriate continuum level for a band, calling for the exercise of some artistic license. Minimum fractional coverages estimated for various ices using this scheme are tabulated in Table 5, based on the grand average Triton spectrum in Fig. 1.

EDITOR: Please place TABLE 5 near here.

The minimum coverages for all five ices add up to considerably more than 100%, from which we can conclude that some regions must exhibit absorption by more than one ice species. From their similar volatilities and similar longitudinal distributions, we have already proposed that CO and N<sub>2</sub> ices co-occur, and from its wavelength shifts, Triton’s CH<sub>4</sub> must be dissolved in N<sub>2</sub> ice as well. Combining N<sub>2</sub>, CO, and CH<sub>4</sub> within the  $\geq 56\%$  of the projected area required for CH<sub>4</sub> reduces the minimum total to much closer to 100%. Likewise, it would not be unreasonable to expect the non-volatile species H<sub>2</sub>O and CO<sub>2</sub> to co-occur in “bedrock” outcrops. These arguments lead to a picture of Triton’s surface as being composed of two distinct compositional units, a non-volatile bedrock consisting of CO<sub>2</sub> and H<sub>2</sub>O covering at least 30% of the projected area, plus a volatile veneer composed of N<sub>2</sub>, CO, and CH<sub>4</sub> covering at least 56% of the projected area. Comparable scenarios have been proposed previously (e.g., Quirico *et al.* 1999).

The different longitudinal distributions of N<sub>2</sub> and CH<sub>4</sub> and also of CO<sub>2</sub> and H<sub>2</sub>O absorption imply compositional heterogeneity within these two units. In the case of the non-volatile bedrock, the absence of longitudinal variation in the CO<sub>2</sub> absorptions requires a very uniform, or exclusively high-latitude distribution of that ice. But the weak enhancement of H<sub>2</sub>O ice absorption seen on Triton’s leading hemisphere implies additional H<sub>2</sub>O on that hemisphere, possibly excavated from the subsurface or delivered via impacts. For our 28% minimum H<sub>2</sub>O ice coverage, this 12% enhancement in H<sub>2</sub>O absorption on the leading hemisphere would be consistent with 29.6% fractional coverage by H<sub>2</sub>O ice on the leading hemisphere, versus versus 26.4% coverage on the trailing hemisphere. This enhancement corresponds to a minimum increased H<sub>2</sub>O coverage on the leading hemisphere of 3.2% of Triton’s projected area, or at least an additional  $1.8 \times 10^5$  km<sup>2</sup> near the sub-Earth point (more, if located away from the center of the visible disk). This additional H<sub>2</sub>O ice rich area on the leading hemisphere need not be recognizably cratered. It could simply feature very fine H<sub>2</sub>O ice ejecta, perhaps even redistributed from its point of origin as

wind-blown dust.

The situation of the volatile compositional unit is more complex. With its  $\geq 56\%$  coverage,  $\text{CH}_4$  ice must be very widely distributed. Its blue-shifted absorption bands imply it is generally dissolved in  $\text{N}_2$  ice, yet the longitudinal distribution of the  $\text{N}_2$  ice absorption implies the nitrogen producing this absorption is distributed over a much smaller fraction of Triton’s visible surface. Both  $\text{N}_2$  distribution models shown in Fig. 11 cover considerably less than 56% of the visible face of Triton. The implication is that some regions which contain both  $\text{N}_2$  and  $\text{CH}_4$  ices are not contributing appreciably to the observed  $2.15 \mu\text{m}$   $\text{N}_2$  ice absorption band but are contributing  $\text{CH}_4$  absorption.  $\text{N}_2$  ice will be spectrally invisible if its particle size is small enough (mm or smaller), or if it contains abundant small scattering inclusions of another ice with a contrasting refractive index (or even of void space, e.g., Eluszkiewicz and Moncet 2003). Such a situation might result from incorporation of wind-blown dust particles of a non-volatile such as  $\text{CO}_2$  ice, with refractive index  $n = 1.4$  (Hansen 1997; Grundy *et al.* 2002b), or of incomplete or hindered densification (Eluszkiewicz *et al.* 2007). It could also occur if the temperature-dependent solubility of  $\text{CH}_4$  in  $\text{N}_2$  triggers exsolution of tiny methane-rich crystals, with  $n \approx 1.3$  (Pearl *et al.* 1991). The presence of spectrally invisible  $\text{N}_2$  ice has important implications for Triton’s atmosphere which we will discuss in a future paper. More widespread  $\text{N}_2$  ice would intercept more sunlight and thus could support higher atmospheric pressures. It would also help to explain the presence of geysers discovered by Voyager II in Triton’s South polar regions (Soderblom *et al.* 1990) and thought to be driven by sublimation of  $\text{N}_2$  (Kirk *et al.* 1990), despite these regions apparently not contributing appreciably to the observed  $2.15 \mu\text{m}$   $\text{N}_2$  absorption band.

An additional complexity of the volatile compositional unit is the observed trend of decreasing longitudinal variability from weak to strong  $\text{CH}_4$  bands illustrated in Figs. 3

and 4 and Table 3. As discussed earlier, a possible explanation could be the existence of relatively localized regions around  $300^\circ$  longitude having large optical path lengths in  $\text{CH}_4$ . From the shallow depths of the weak  $\text{CH}_4$  bands ( $\sim 5\%$  for the  $0.89 \mu\text{m}$  band), these regions of enhanced  $\text{CH}_4$  absorption need not cover much of Triton’s surface. They would contribute to the absorption in all of the  $\text{CH}_4$  bands, but their spectral effect would be most evident in the weakest  $\text{CH}_4$  bands which are almost too weak to detect in models fitted to the strongest  $\text{CH}_4$  bands (the stronger bands require far shorter mean optical path lengths in  $\text{CH}_4$ ). If these hypothetical regions of greater  $\text{CH}_4$  path length are comparatively depleted in  $\text{N}_2$  ice, their  $\text{CH}_4$  bands will be less blue-shifted than in other regions. This would lead to longitude-dependent shifts in the  $\text{CH}_4$  bands, with minimum shifts coinciding with the longitudes of these regions. Such a pattern is exactly what we have observed, as plotted in Fig. 5. Unfortunately, we do not have enough information to be able to link these anomalously  $\text{CH}_4$ -rich regions to specific areas in Voyager images, which might have enabled us to use their geomorphology to infer whether they are sources of new  $\text{CH}_4$  escaping from Triton’s deep interior, or are lag deposits produced by preferential sublimation loss of the more volatile  $\text{N}_2$  ice.

## 6. Conclusion

Near-infrared spectra of Triton show distinct longitudinal variation patterns for absorptions by  $\text{N}_2$ ,  $\text{CO}$ ,  $\text{CH}_4$ ,  $\text{CO}_2$ , and  $\text{H}_2\text{O}$  ices. These variations have persisted over the nine years covered by our observations. They have important implications for the spatial distributions of Triton’s different ice species:

- Nitrogen ice absorption shows very pronounced oscillation as Triton rotates, being strongest on the leading side of the Neptune-facing hemisphere. This pattern is consistent with a simple thermal balance model. It is also consistent with a subset of

the McEwen (1990) color units, but only if the  $N_2$  is confined to parts of those units far from Triton’s South pole. There is evidence for ongoing seasonal loss of  $N_2$  ice from Triton’s summer hemisphere.

- Carbon monoxide absorption is strongest where nitrogen absorption is strongest. The very similar patterns of longitudinal variation, similar volatilities, and miscibility of CO in  $N_2$  ice imply co-occurrence.
- Methane ice absorption is distributed very differently from  $N_2$  and CO absorption, being strongest on the Neptune-facing side of Triton’s trailing hemisphere. Weaker methane ice absorptions which probe more deeply into Triton’s surface show stronger longitudinal variation than the stronger methane ice bands do. Wavelength shifts of methane bands indicate that the methane is diluted in nitrogen ice, but the dilution is slightly less where the methane absorptions are strongest.
- Although Triton’s methane is diluted in nitrogen ice, the large fraction of Triton’s visible area required to produce the strongest  $CH_4$  absorption bands is inconsistent with the small fraction of the visible area needed to explain the larger longitudinal variation in the  $N_2$  ice band. We conclude that some of Triton’s mixed  $N_2+CH_4$  ice is not contributing appreciably to the observed  $2.15 \mu\text{m}$   $N_2$  band, perhaps because its texture produces relatively short mean optical path lengths. If CO co-occurs with this spectrally-hidden  $N_2$  ice, it too must be hidden in order to match the longitudinal variation of the  $N_2$ .
- Water ice absorption is slightly stronger on Triton’s leading hemisphere, as is seen on many other icy satellites.
- Carbon dioxide ice absorption is remarkably static as Triton rotates, implying a globally homogeneous and/or exclusively high-latitude distribution.

We intend to continue our near-infrared spectral observations of Triton into the future, in order to better resolve seasonal effects and to continue the search for transient behavior. As one of several small outer Solar System bodies with seasonally active volatile ices, these observations will help us understand the growing family which now includes Pluto, Eris, and Makemake. Perhaps others, as-yet undiscovered, will soon be added to their ranks, further boosting the prospects for comparative planetology of these strange, icy worlds.

ACKNOWLEDGMENTS: We are grateful to W. Golisch, D. Griep, P. Sears, E. Volquardsen, S.J. Bus, and J.T. Rayner for assistance with the IRTF and with SpeX, and to NASA for its support of the IRTF. We thank M.R. Showalter for the Rings Node’s on-line ephemeris services, and also NASA’s Jet Propulsion Laboratory for the Horizons on-line ephemeris services. We also thank the free and open source software communities for empowering us with the software used to complete this project, notably Linux, the GNU tools, L<sup>A</sup>T<sub>E</sub>X, FVWM, Tcl/Tk, Python, Evolution, and MySQL. We recognize the cultural significance of the summit of Mauna Kea within the indigenous Hawaiian community and are grateful for the opportunity to observe from this site. This work was funded by NSF grants AST-0407214 and AST-0085614 and by NASA grants NAG5-4210, NAG5-10497, NAG5-12516, and NNG04G172G.

## REFERENCES

- Abernathy, M.R., S.C. Tegler, W.M. Grundy, J. Licandro, W. Romanishin, D. Cornelison, and F. Vilas 2009. Digging into the surface of the icy dwarf planet Eris. *Icarus* **199**, 520-525.
- Brown Jr., G.N., and W.T. Ziegler 1980. Vapor pressure and heats of vaporization and sublimation of liquids and solids of interest in cryogenics below 1-atm pressure. *Adv. Cryogenic Eng.* **25**, 662-670.
- Brunetto, R., G. Caniglia, G.A. Baratta, and M.E. Palumbo 2008. Integrated near-infrared band strengths of solid CH<sub>4</sub> and its mixtures with N<sub>2</sub>. *Astrophys. J.* **686**, 1480-1485.
- Buratti, B.J., J.D. Goguen, J. Gibson, and J. Mosher 1994. Historical photometric evidence for volatile migration on Triton. *Icarus* **110**, 303-314.
- Buratti, B.J., M.D. Hicks, and R.L. Newburn Jr. 1999. Does global warming make Triton blush? *Nature* **397**, 219-220.
- Bus, S.J., A.J. Denault, J.T. Rayner, R.P. Binzel, and M. Bîrlan 2002. Remote observing at the NASA Infrared Telescope Facility (IRTF). *SPIE* **4845**, 94-99.
- Cornelison, D.M., S.C. Tegler, W. Grundy, and M. Abernathy 2008. Near-infrared laboratory spectroscopy of CH<sub>4</sub>/N<sub>2</sub> ice mixtures: Implications for icy dwarf planets. Paper presented at *The Science of Solar System Ices (ScSSI): A cross-disciplinary workshop*, Oxnard CA, 2008 May 5-8.
- Croft, S.K., J.S. Kargel, R.L. Kirk, J.M. Moore, P.M. Schenk, and R.G. Strom 1995. The geology of Triton. In *Neptune and Triton*, Ed. D.P. Cruikshank, Univ. of Arizona Press, Tucson.

- Elliot, J.L., M.J. Person, S.W. McDonald, M.W. Buie, E.W. Dunham, R.L. Millis, R.A. Nye, C.B. Olkin, L.H. Wasserman, L.A. Young, W.B. Hubbard, R. Hill, H.J. Reitsema, J.M. Pasachoff, T.H. McConnochie, B.A. Babcock, R.C. Stone, and P. Francis 2000. The prediction and observation of the 1997 July 18 stellar occultation by Triton: More evidence for distortion and increasing pressure in Triton’s atmosphere. *Icarus* **148**, 347-369.
- Eluszkiewicz, E., and J.L. Moncet 2003. A coupled microphysical/radiative transfer model of albedo and emissivity of planetary surfaces covered by volatile ices. *Icarus* **166**, 375-384.
- Eluszkiewicz, E., K. Cady-Pereira, M.E. Brown, and J.A. Stansberry 2007. Interpretation of the near-IR spectra of the Kuiper belt object (136472) 2005 FY<sub>9</sub>. *J. Geophys. Res.* **112**, E06003.1-8.
- Grundy, W.M., B. Schmitt, and E. Quirico 1993. The temperature dependent spectra of  $\alpha$  and  $\beta$  nitrogen ice with application to Triton. *Icarus* **105**, 254-258.
- Grundy W.M., M.W. Buie, J.A. Stansberry, J.R. Spencer, and B. Schmitt 1999. Near-infrared spectra of icy outer solar system surfaces: Remote determination of H<sub>2</sub>O ice temperatures. *Icarus* **142**, 536-549.
- Grundy W.M., B. Schmitt, and E. Quirico 2002a. The temperature dependent spectrum of methane ice I between 0.65 and 5 microns and opportunities for near-infrared remote thermometry. *Icarus* **155**, 486-496.
- Grundy, W.M., M.W. Buie, and J.R. Spencer 2002b. Spectroscopy of Pluto and Triton at 3-4 microns: Possible evidence for wide distribution of nonvolatile solids. *Astron. J.* **124**, 2273-2278.

- Grundy, W.M., L.A. Young, J.R. Spencer, R.E. Johnson, E.F. Young, and M.W. Buie 2006. Distributions of H<sub>2</sub>O and CO<sub>2</sub> ices on Ariel, Umbriel, Titania, and Oberon from IRTF/SpEX observations. *Icarus* **184**, 543-555.
- Grundy, W.M., and U. Fink 1996. Synoptic CCD spectrophotometry of Pluto over the past 15 years. *Icarus* **124**, 329-343.
- Grundy, W.M., and J.A. Stansberry 2000. Solar gardening and the seasonal evolution of nitrogen ice on Triton and Pluto. *Icarus* **148**, 340-346.
- Grundy, W.M., and L.A. Young 2004. Near infrared spectral monitoring of Triton with IRTF/SpEX I: Establishing a baseline. *Icarus* **172**, 455-465.
- Hansen, C.J., and D.A. Paige 1992. A thermal model for the seasonal nitrogen cycle on Triton. *Icarus* **99**, 273-288.
- Hansen, G.B. 1997. The infrared absorption spectrum of carbon dioxide ice from 1.8 to 333 microns. *J. Geophys. Res.* **102**, 21569-21587.
- Hicks, M.D., and B.J. Buratti 2004. The spectral variability of Triton from 1997-2000. *Icarus* **171**, 210-218.
- Houk, N., and M. Smith-Moore 1988. *Catalogue of two-dimensional spectral types for the HD stars. Vol. 4*. Dept. of Astronomy, Univ. of Michigan, Ann Arbor MI.
- Kirk, R.L., R.H. Brown, and L.A. Soderblom 1990. Subsurface energy storage and transport for solar-powered geysers on Triton. *Science* **250**, 424-429.
- Licandro, J., W.M. Grundy, N. Pinilla-Alonso, and P. Leysi 2006. Visible spectroscopy of TNO 2003 UB<sub>313</sub>: Evidence for N<sub>2</sub> ice on the surface of the largest TNO? *Astron. & Astrophys.* **458**, L5-L8.

- Lunine, J.I., and D.J. Stevenson 1985. Physical state of volatiles on the surface of Triton. *Nature* **317**, 238-240.
- McEwen, A.S. 1990. Global color and albedo variations on Triton. *Geophys. Res. Lett.* **17**, 1765-1768.
- Merlin, F., A. Alvarez-Candal, A. Delsanti, S. Fornasier, M.A. Barucci, F.E. DeMeo, C. de Bergh, A. Doressoundiram, E. Quirico, and B. Schmitt 2009. Stratification of methane ice on Eris’ surface. *Astron. J.* **137**, 315-328.
- Neckel, H. 1986. The “bright stars” with UBV-colors close to those of the Sun. *Astron. & Astrophys.* **169**, 194-200.
- Owen, T.C., T.L. Roush, D.P. Cruikshank, J.L. Elliot, L.A. Young, C. de Bergh, B. Schmitt, T.R. Geballe, R.H. Brown, and M.J. Bartholomew 1993. Surface ices and atmospheric composition of Pluto. *Science* **261**, 745-748.
- Pearl, J., M. Ngoh, M. Ospina, and R. Khanna 1991. Optical constants of solid methane and ethane from 10,000 to 450  $\text{cm}^{-1}$ . *J. Geophys. Res.* **96**, 17477-17482.
- Pourbaix, D., A.A. Tokovinin, A.H. Batten, F.C. Fekel, W.I. Hartkopf, H. Levato, N.I. Morrell, G. Torres, and S. Udry 2004.  $S_B^9$ : The ninth catalogue of spectroscopic binary orbits. *Astron. & Astrophys.* **424**, 727-732.
- Prokhvatilov, A.I., and L.D. Yantsevich 1983. X-ray investigation of the equilibrium phase diagram of  $\text{CH}_4\text{-N}_2$  solid mixtures. *Sov. J. Low Temp. Phys.* **9**, 94-98.
- Quirico, E., and B. Schmitt 1997. Near-infrared spectroscopy of simple hydrocarbons and carbon oxides diluted in solid  $\text{N}_2$  and as pure ices: Implications for Triton and Pluto. *Icarus* **127**, 354-378.

- Quirico, E., S. Douté, B. Schmitt, C. de Bergh, D.P. Cruikshank, T.C. Owen, T.R. Geballe, and T.L. Roush 1999. Composition, physical state, and distribution of ices at the surface of Triton. *Icarus* **139**, 159-178.
- Rayner, J.T., D.W. Toomey, P.M. Onaka, A.J. Denault, W.E. Stahlberger, D.Y. Watanabe, and S.I. Wang 1998. SpeX: A medium-resolution IR spectrograph for IRTF. *Proc. SPIE* **3354**, 468-479.
- Rayner, J.T., D.W. Toomey, P.M. Onaka, A.J. Denault, W.E. Stahlberger, W.D. Vacca, M.C. Cushing, and S. Wang 2003. SpeX: A medium-resolution 0.8–5.5 micron spectrograph and imager for the NASA Infrared Telescope Facility. *Publ. Astron. Soc. Pacific* **115**, 362-382.
- Schenk, P.M., and K. Zahnle 2007. On the negligible surface age of Triton. *Icarus* **192**, 135-149.
- Scott, T.A. 1976. Solid and liquid nitrogen. *Phys. Rep.* **27**, 89-157.
- Soderblom, L.A., S.W. Kieffer, T.L. Becker, R.H. Brown, A.F. Cook II, C.J. Hansen, T.V. Johnson, R.L. Kirk, and E.M. Shoemaker 1990. Triton's geyser-like plumes: Discovery and basic characterization. *Science* **250**, 410-415.
- Spencer, J.R., and J.M. Moore 1992. The influence of thermal inertia on temperatures and frost stability on Triton. *Icarus* **99**, 261-272.
- Stansberry, J.A., R.V. Yelle, J.I. Lunine, and A.S. McEwen 1992. Triton's surface-atmosphere energy balance. *Icarus* **99**, 242-260.
- Stern, S.A., and W.B. McKinnon 2000. Triton's surface age and impactor population revisited in light of Kuiper belt fluxes: Evidence for small Kuiper belt objects and recent geological activity. *Astron. J.* **119**, 945-952.

- Tegler, S.C., W.M. Grundy, F. Vilas, W. Romanishin, D. Cornelison, and G.J. Consolmagno, S.J. 2008. Evidence of N<sub>2</sub>-ice on the surface of the icy dwarf planet 136472 (2005 FY<sub>9</sub>). *Icarus* **195**, 844-850.
- Trafton, L.M., D.L. Matson, and J.A. Stansberry 1998. Surface/atmosphere interactions and volatile transport (Triton, Pluto, and Io). In *Solar System Ices*, Eds. B. Schmitt, C. de Bergh, and M. Festou, Kluwer Academic, Boston, 773-812.
- Tryka, K.A., R.H. Brown, V. Anicich, D.P. Cruikshank, and T.C. Owen 1993. Spectroscopic determination of the phase composition and temperature of nitrogen ice on Triton. *Science* **261**, 751-754.
- Young, L.A., and S.A. Stern 2001. Ultraviolet observations of Triton in 1999 with the Space Telescope Imaging Spectrograph: 2150-3180 Å spectroscopy and disk-integrated photometry. *Astron. J.* **122**, 449-456.
- Zahnle, K., P. Schenk, S. Sobieszczyk, L. Dones, and H.F. Levison 2001. Differential cratering of synchronously rotating satellites by ecliptic comets. *Icarus* **153**, 111-129.
- Zahnle, K., P. Schenk, H. Levison, and L. Dones 2003. Cratering rates in the outer solar system. *Icarus* **163**, 263-289.

Table 1. Circumstances of observations

UT date of observation mean-time	Sky conditions and H band image size	Sub-Earth		Phase angle	Triton integration
		longitude (°E)	latitude (°S)	(°)	(min)
2000/07/22 9:17	Heavy cirrus, 0.8''	344.5	50.0	0.19	9
2001/07/03 11:56	Clouds, 2.5''	310.3	49.9	0.87	47
2001/07/04 12:05	Heavy Cirrus, 1.1''	11.9	49.9	0.84	67
2001/07/05 12:39	Cirrus, 1.1''	74.6	49.9	0.81	48
2001/07/06 12:03	Heavy cirrus, 0.9''	134.3	49.9	0.78	64
2001/07/07 12:07	Cirrus, 1.0''	195.7	49.9	0.75	56
2001/07/08 11:44	Clear, 1.1''	255.9	49.9	0.72	80
2002/07/15 9:24	Clear, 0.6''	0.7	49.8	0.58	52
2002/07/16 9:24	Scattered clouds, 0.7''	61.9	49.8	0.55	54
2002/07/17 9:53	Cirrus, 0.8''	124.3	49.8	0.52	84
2002/07/18 9:36	Thin cirrus, 0.8''	184.8	49.8	0.49	64
2002/07/19 9:31	Thin cirrus, 0.7''	245.8	49.8	0.46	68
2002/07/20 9:27	Thin cirrus, 0.8''	306.9	49.8	0.42	68
2002/07/21 9:29	Thin cirrus, 0.6''	8.2	49.8	0.39	68
2002/07/22 9:21	Clear, 0.7''	69.1	49.8	0.36	84
2002/08/16 11:10	Clouds, 1.0''	164.1	49.9	0.47	96
2002/09/16 6:19	Cirrus, 0.5''	249.5	49.9	1.34	84
2002/10/03 6:32	Unrecorded, 0.6''	211.0	49.9	1.67	48

Table 1—Continued

UT date of observation mean-time	Sky conditions and H band image size	Sub-Earth		Phase angle (°)	Triton integration (min)
		longitude (°E)	latitude (°S)		
2003/07/04 13:58	Clear, 0.5''	101.0	49.6	0.98	64
2003/07/29 11:59	Heavy cirrus, 0.7''	186.5	49.7	0.21	28
2003/08/10 10:09	Some clouds, 0.5''	196.4	49.7	0.19	58
2003/09/10 9:32	Clear, 0.6''	292.6	49.8	1.13	40
2003/10/16 5:51	Patchy clouds, 0.5''	327.5	49.8	1.80	88
2004/06/28 13:07	Cirrus, 0.5''	194.9	49.3	1.19	152
2004/07/28 11:44	Clear, then fog, 0.6''	228.0	49.4	0.29	36
2004/08/12 12:19	Clear, 0.7''	67.7	49.5	0.21	52
2004/09/12 10:51	Clear, 1.0''	161.7	49.6	1.15	48
2004/10/21 6:13	Partly cloudy, 0.8''	18.0	49.6	1.84	52
2005/07/04 13:06	Clear, 0.7''	244.3	48.9	1.10	146
2005/08/01 10:22	Cirrus, 0.6''	151.5	49.1	0.25	44
2005/08/04 9:53	Cirrus, 0.7''	333.9	49.1	0.15	76
2005/09/19 8:02	Clear, 0.5''	265.2	49.3	1.26	68
2006/05/26 14:52	Clear, 0.4''	62.3	48.4	1.86	40
2006/06/26 13:39	Cirrus, 0.4''	157.9	48.5	1.37	128
2006/07/26 11:01	Clear, 0.9''	188.0	48.6	0.53	72
2006/08/30 9:14	Clear, 0.7''	166.0	48.8	0.62	48

Table 1—Continued

UT date of observation mean-time	Sky conditions and H band image size	Sub-Earth		Phase angle (°)	Triton integration (min)
		longitude (°E)	latitude (°S)		
2006/10/28 5:59	Thin cirrus, 0.6''	170.3	49.0	1.85	68
2007/06/21 13:15	Clear, 0.8''	252.6	47.9	1.53	136
2007/06/22 13:10	Thin cirrus, 0.6''	313.7	47.9	1.51	160
2007/06/23 13:18	Clear, 0.6''	15.2	47.9	1.49	128
2007/06/24 14:06	Clear, 0.7''	78.5	47.9	1.47	88
2007/06/25 13:13	Clear, 0.5''	137.5	47.9	1.45	132
2007/06/26 13:09	Heavy cirrus, 0.7''	198.6	47.9	1.43	172
2007/06/27 13:16	Humid, 1.2''	260.1	47.9	1.41	132
2007/08/01 11:59	Clear, 0.9''	239.8	48.1	0.41	16
2008/06/24 14:36	Clear, 0.5''	182.9	47.3	1.50	56
2008/07/14 10:57	Clear, 0.5''	318.3	47.4	1.01	72
2008/08/12 12:24	Clear, 0.9''	297.5	47.6	0.10	44
2008/09/01 7:02	Clear, 0.6''	68.1	47.8	0.55	56
2008/09/28 9:55	Partly cloudy, 0.5''	288.5	48.0	1.32	60

Table 2. Wavelengths ( $\mu\text{m}$ ) used for computing integrated areas of absorption bands

Absorption band	Continuum	Band	Continuum
$\text{N}_2$ 2.15 $\mu\text{m}$	2.093 - 2.117	2.117 - 2.175	2.175 - 2.185
$\text{CH}_4$ 0.89 $\mu\text{m}$	0.860 - 0.878	0.878 - 0.909	0.909 - 0.930
$\text{CH}_4$ 1.15 $\mu\text{m}$	1.070 - 1.100	1.100 - 1.210	1.210 - 1.230
$\text{CH}_4$ 1.33 $\mu\text{m}$	1.300 - 1.310	1.310 - 1.342	1.342 - 1.348
$\text{CH}_4$ 1.65 $\mu\text{m}$	1.605 - 1.620	1.620 - 1.685	1.685 - 1.699
$\text{CH}_4$ 1.73 $\mu\text{m}$	1.686 - 1.698	1.698 - 1.735	1.735 - 1.745
$\text{CH}_4$ 2.20 $\mu\text{m}$	2.170 - 2.180	2.180 - 2.225	2.225 - 2.235
$\text{CO}_2$ 1.965 $\mu\text{m}$	1.957 - 1.962	1.962 - 1.969	1.969 - 1.974
$\text{CO}_2$ 2.01 $\mu\text{m}$	2.002 - 2.008	2.008 - 2.015	2.015 - 2.020
$\text{CO}_2$ 2.07 $\mu\text{m}$	2.062 - 2.068	2.068 - 2.072	2.072 - 2.078
$\text{CO}$ 2.35 $\mu\text{m}$	2.338 - 2.343	2.343 - 2.356	2.356 - 2.362

Table 3. Sinusoidal fits to longitudinal variations of Triton’s absorption bands

Absorption band	Peak-to-peak amplitude (%)	East longitude of maximum ( $^{\circ}$ )
N <sub>2</sub> 2.15 $\mu\text{m}$	$76 \pm 4$	$31 \pm 3$
CO 2.35 $\mu\text{m}$	$71 \pm 7$	$58 \pm 5$
CH <sub>4</sub> 0.89 $\mu\text{m}$	$34 \pm 6$	$282 \pm 10$
CH <sub>4</sub> 1.15 $\mu\text{m}$	$33 \pm 7$	$304 \pm 12$
CH <sub>4</sub> 1.33 $\mu\text{m}$	$23 \pm 10$	$297 \pm 28$
CH <sub>4</sub> 1.65 $\mu\text{m}$	$15 \pm 1$	$317 \pm 3$
CH <sub>4</sub> 1.73 $\mu\text{m}$	$21 \pm 2$	$321 \pm 5$
CH <sub>4</sub> 2.20 $\mu\text{m}$	$20 \pm 2$	$299 \pm 7$
H <sub>2</sub> O ratio	$12 \pm 3$	$119 \pm 14$
CO <sub>2</sub> triplet	$2 \pm 2$	$231 \pm 18$

Table 4. N<sub>2</sub> distributions tied to McEwen (1990) color units

Units having N <sub>2</sub> ice	Latitude cut off (°)	Band area ( $\mu\text{m}$ )	Goodness of fit $\chi^2_\nu$
0,2,5	–31	0.017	1.13
2,5	–34	0.015	1.30
2,3,5,6	–24	0.016	1.60
0,2,3,5,6	–22	0.017	2.05
0,2,3,5	–31	0.016	2.26
2,3,4,5,6	–13	0.021	2.44
2,3,5	–35	0.014	2.71

Note. — Unit 0 represents regions not assigned a unit number by McEwen (1990).

Table 5. Estimated minimum fractional coverage for each ice

Ice species	Minimum fractional coverage	Absorption band used in estimation
N <sub>2</sub>	18%	2.15 $\mu\text{m}$
CO	27%	2.35 $\mu\text{m}$
CH <sub>4</sub>	56%	2.32 $\mu\text{m}$
CO <sub>2</sub>	30%	2.01 $\mu\text{m}$
H <sub>2</sub> O	28%	2 $\mu\text{m}$

## FIGURE CAPTIONS

Fig. 1.— Average IRTF/SpeX spectrum of Triton. Vibrational absorptions by various ice species are labeled. These are generally overtones and combinations of longer wavelength fundamental modes. Gaps around 1.4 and 1.9  $\mu\text{m}$  coincide with higher opacity in the terrestrial atmosphere.

Fig. 2.— Integrated area of the 2.15  $\mu\text{m}$   $\text{N}_2$  ice absorption band as a function of sub-Earth longitude on Triton, showing a large periodic variation as Triton rotates. A logarithmic scale is used to facilitate comparison with similar plots to be shown for other ice species. Each point represents observations from a single night, with points duplicated over an additional 180° to better show the cyclic pattern. The dotted curve is a sinusoid fitted to the data.

Fig. 3.— Integrated areas of three  $\text{CH}_4$  ice absorption bands as a function of sub-Earth longitude on Triton, showing periodic variations as Triton rotates. Other features are as described in Fig. 2.

Fig. 4.— Fractional longitudinal variation of six  $\text{CH}_4$  ice absorption bands (labeled according to their wavelengths) as a function of average albedo across the band. In general, weaker bands with higher average albedos sample deeper within the surface. These weaker bands show greater longitudinal variation. The 1.65  $\mu\text{m}$   $\text{CH}_4$  band coincides with a water ice band, which may reduce its apparent variability, since  $\text{H}_2\text{O}$  absorption is stronger on the leading hemisphere, as will be discussed shortly.

Fig. 5.— Average blue shift of Triton’s 1.65, 1.73, and 2.2  $\mu\text{m}$   $\text{CH}_4$  ice absorption bands, relative to the shifts reported by Quirico and Schmitt (1997) for  $\text{CH}_4$  molecules isolated in  $\text{N}_2$  ice. In this plot, a value of zero would correspond to pure  $\text{CH}_4$  ice while a value of one indicates ice in which each  $\text{CH}_4$  molecule has exclusively  $\text{N}_2$  molecules for neighbors. However, a value of 0.9 should not be interpreted as necessarily implying a 90%  $\text{N}_2$  and 10%  $\text{CH}_4$  composition, since the dependence of the shift on concentration is not yet well understood (Cornelison *et al.* 2008; Brunetto *et al.* 2008).  $\text{CH}_4$  is not even soluble in  $\text{N}_2$  ice at 10% concentration, so at least two distinct phases would have to be present at that composition (Prokhvatilov and Yantsevich 1983; Lunine and Stephenson 1985).

Fig. 6.— Fractional band depth of  $\text{H}_2\text{O}$  ice as a function of sub-Earth longitude on Triton, showing a subtle enhancement of  $\text{H}_2\text{O}$  ice absorption on the leading hemisphere ( $12\pm 3\%$  peak-to-peak from the sinusoidal fit shown as a dotted curve).

Fig. 7.— Total integrated area of three narrow  $\text{CO}_2$  ice absorption bands near 2  $\mu\text{m}$  as a function of sub-Earth longitude on Triton, showing no significant evidence of longitudinal variability ( $2\pm 2\%$  peak-to-peak from the sinusoidal fit shown as a dotted curve).

Fig. 8.— Integrated area of the narrow  $\text{CO}$  ice absorption band at 2.352  $\mu\text{m}$  as a function of sub-Earth longitude on Triton, showing a very similar pattern to that of  $\text{N}_2$  ice.

Fig. 9.— Triton’s observed longitudinal spectral variations shown on a consistent logarithmic scale of relative variation.

Fig. 10.— Integrated area of the  $2.15\ \mu\text{m}$   $\text{N}_2$  ice absorption band split into two 4.5-year time periods. In both panels, the solid curve is a sinusoidal fit to just the data taken during that interval, while the dashed curve is a fit to the full 9-year data set (also shown in Figs. 2 and 9).

Fig. 11.— Two models for the spatial distribution of Triton’s  $\text{N}_2$  ice in South polar projection, with areas free of  $\text{N}_2$  ice shown in black and areas covered with  $\text{N}_2$  shown in white. Longitude and latitude lines are at  $30^\circ$  intervals. The bottom panel shows the longitudinal variation in the  $\text{N}_2$  integrated area, as in Fig. 2. The black curves show the behavior of the McEwen units model (dashed) and the thermal balance model (solid). Gray versions of these curves show how the two models might respond to seasonal recession of  $\text{N}_2$  ice coverage.

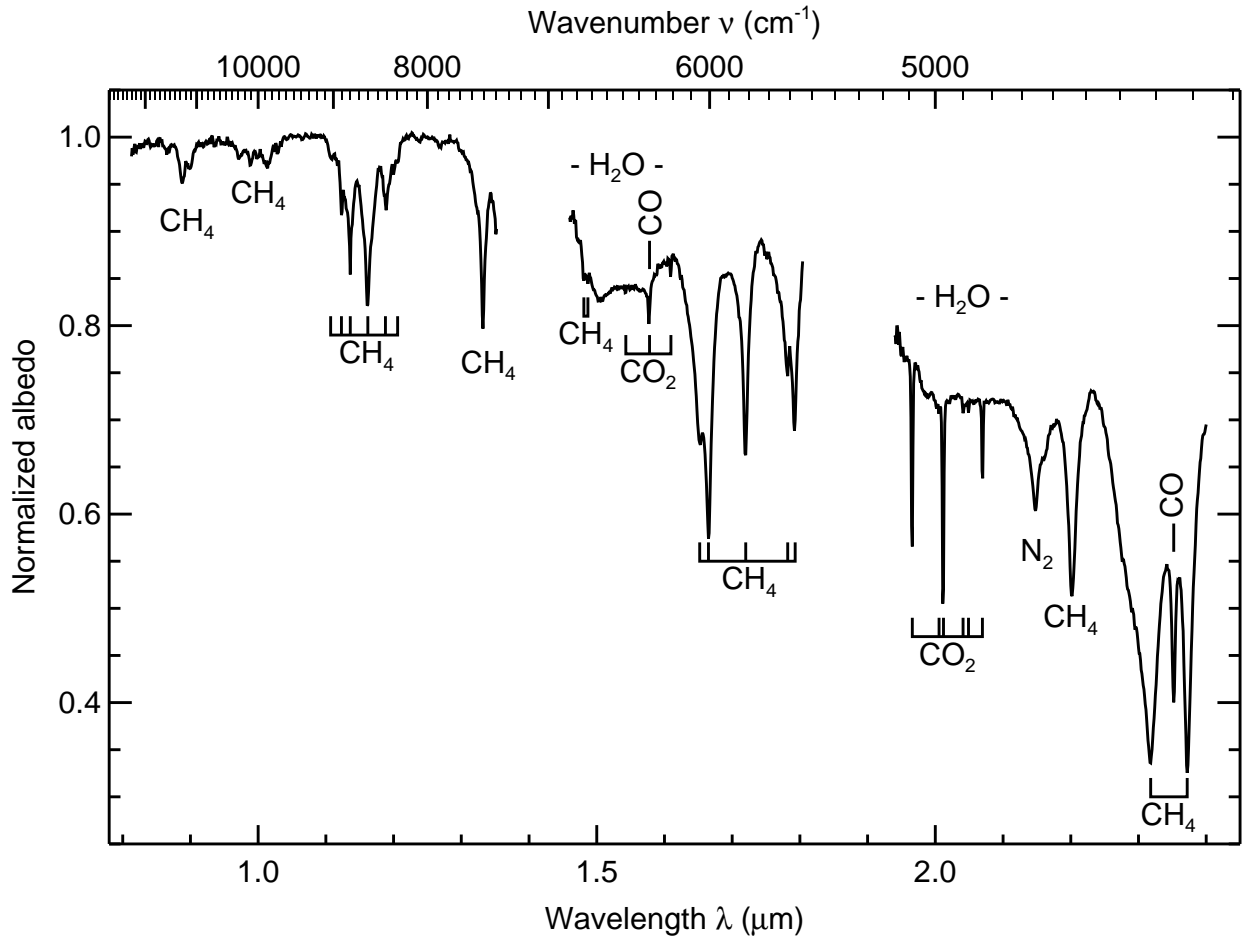


Fig. 1.— Average IRTF/SpeX spectrum of Triton. Vibrational absorptions by various ice species are labeled. These are generally overtones and combinations of longer wavelength fundamental modes. Gaps around 1.4 and 1.9  $\mu\text{m}$  coincide with higher opacity in the terrestrial atmosphere.

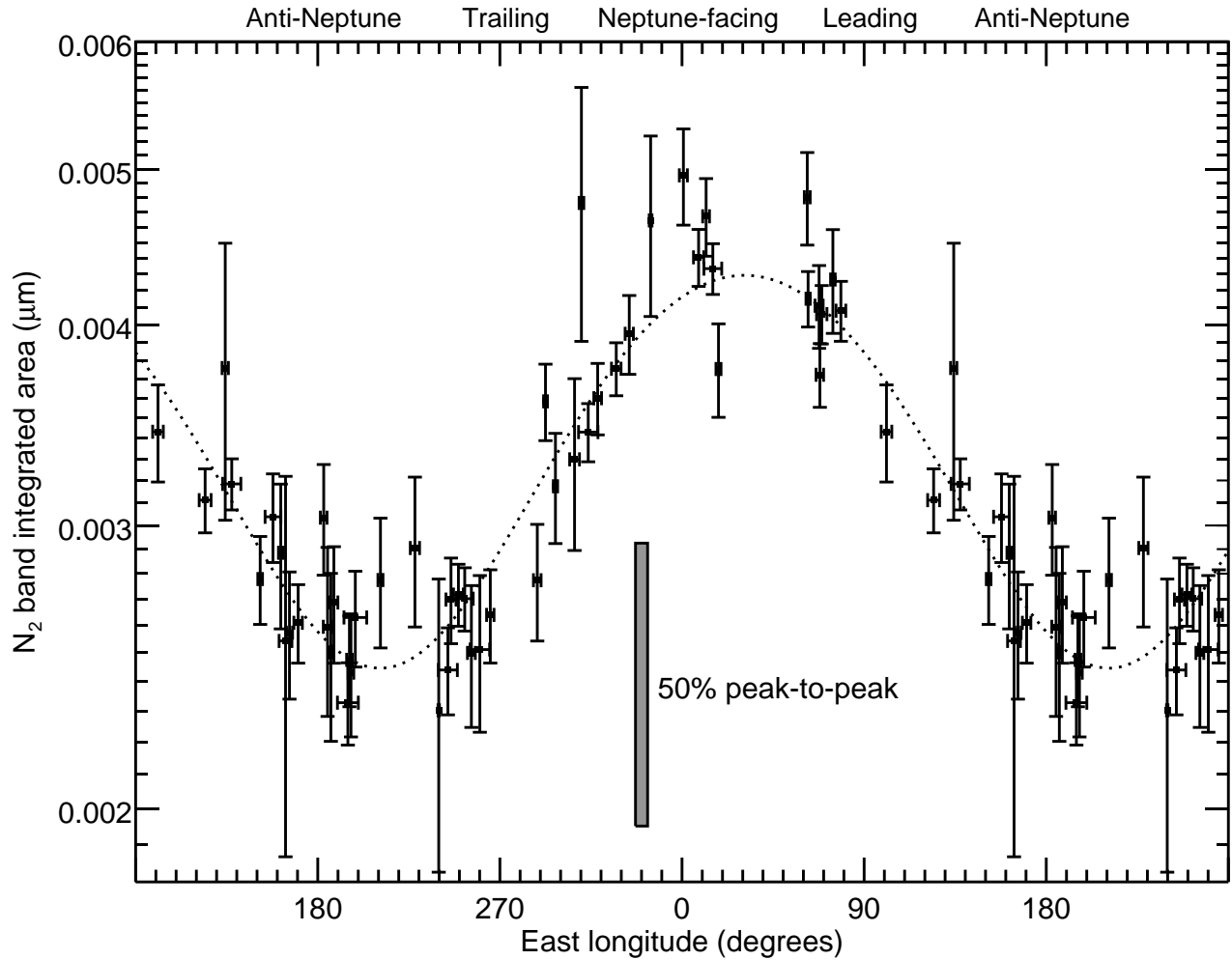


Fig. 2.— Integrated area of the  $2.15 \mu\text{m}$   $\text{N}_2$  ice absorption band as a function of sub-Earth longitude on Triton, showing a large periodic variation as Triton rotates. A logarithmic scale is used to facilitate comparison with similar plots to be shown for other ice species. Each point represents observations from a single night, with points duplicated over an additional  $180^\circ$  to better show the cyclic pattern. The dotted curve is a sinusoid fitted to the data.

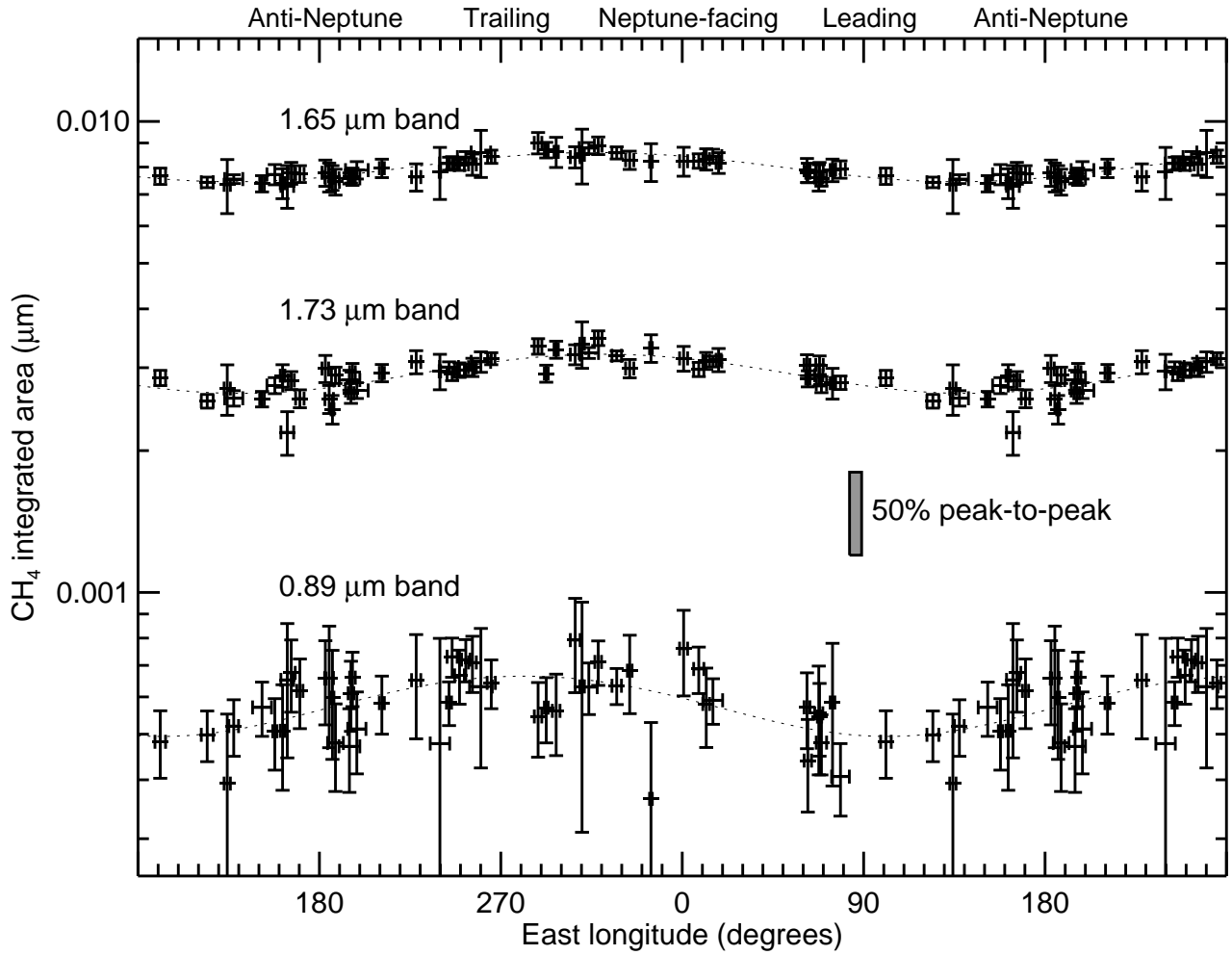


Fig. 3.— Integrated areas of three CH<sub>4</sub> ice absorption bands as a function of sub-Earth longitude on Triton, showing periodic variations as Triton rotates. Other features are as described in Fig. 2.

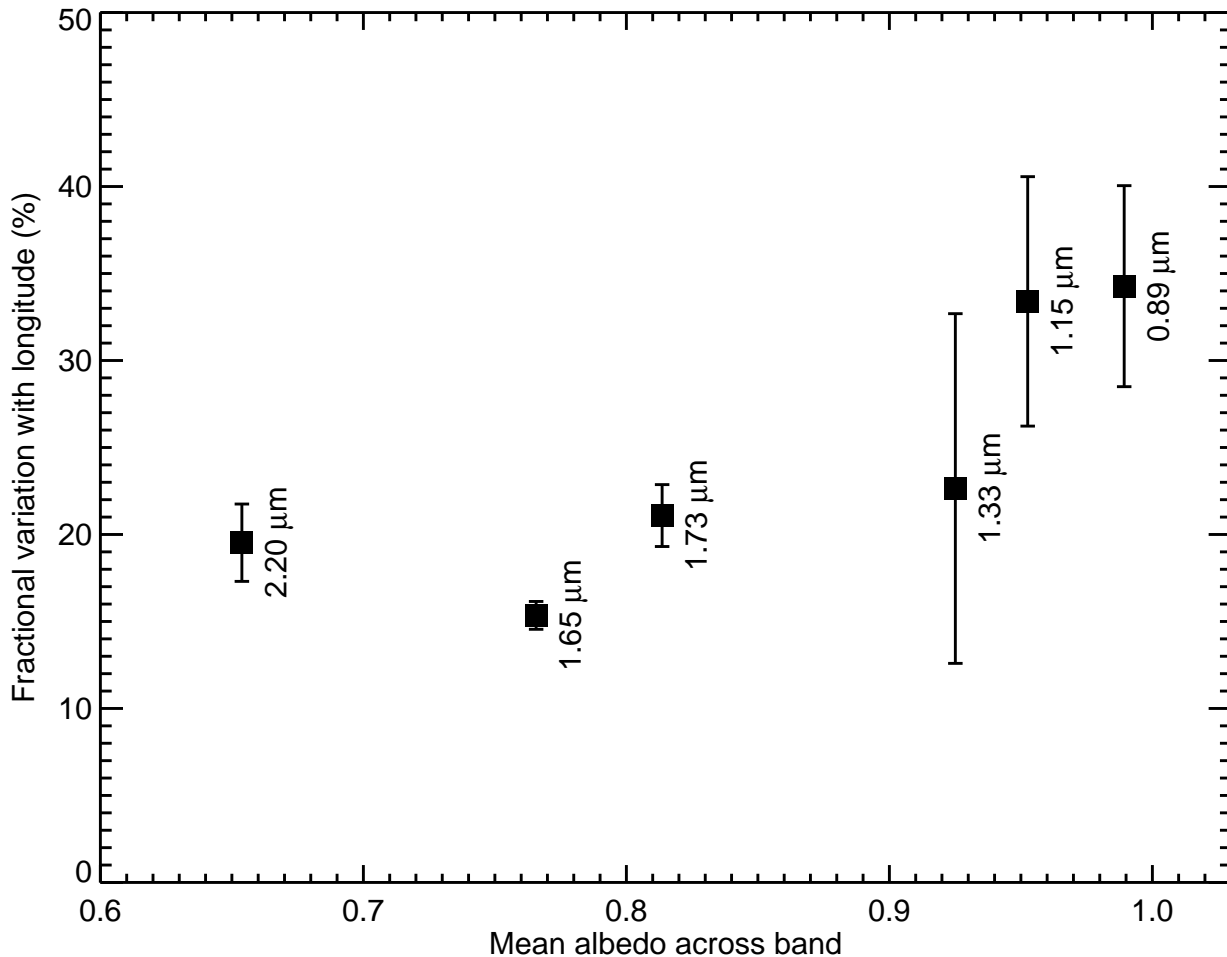


Fig. 4.— Fractional longitudinal variation of six  $\text{CH}_4$  ice absorption bands (labeled according to their wavelengths) as a function of average albedo across the band. In general, weaker bands with higher average albedos sample deeper within the surface. These weaker bands show greater longitudinal variation. The  $1.65 \mu\text{m}$   $\text{CH}_4$  band coincides with a water ice band, which may reduce its apparent variability, since  $\text{H}_2\text{O}$  absorption is stronger on the leading hemisphere, as will be discussed shortly.

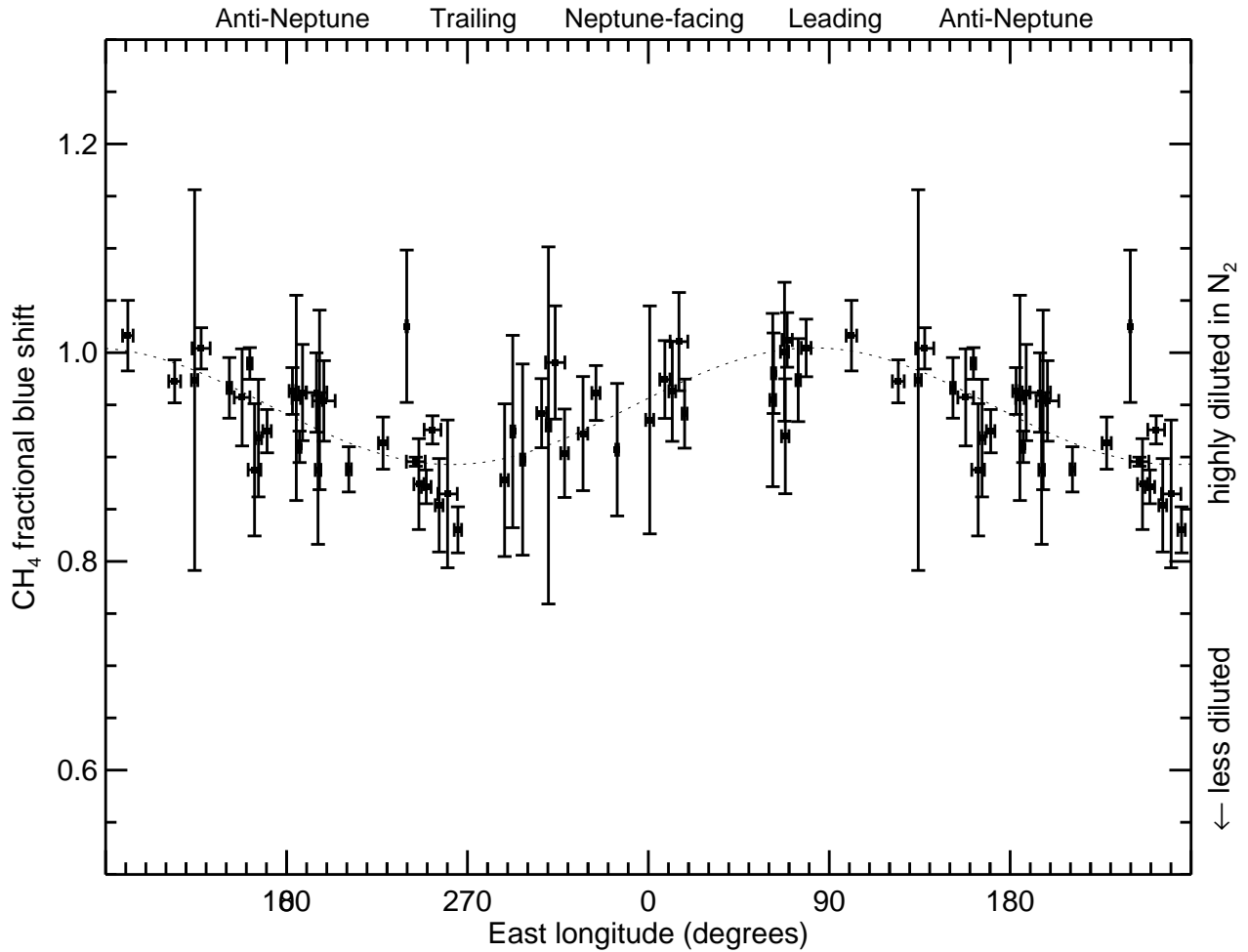


Fig. 5.— Average blue shift of Triton’s 1.65, 1.73, and 2.2  $\mu\text{m}$   $\text{CH}_4$  ice absorption bands, relative to the shifts reported by Quirico and Schmitt (1997) for  $\text{CH}_4$  molecules isolated in  $\text{N}_2$  ice. In this plot, a value of zero would correspond to pure  $\text{CH}_4$  ice while a value of one indicates ice in which each  $\text{CH}_4$  molecule has exclusively  $\text{N}_2$  molecules for neighbors. However, a value of 0.9 should not be interpreted as necessarily implying a 90%  $\text{N}_2$  and 10%  $\text{CH}_4$  composition, since the dependence of the shift on concentration is not yet well understood (Cornelison *et al.* 2008; Brunetto *et al.* 2008).  $\text{CH}_4$  is not even soluble in  $\text{N}_2$  ice at 10% concentration, so at least two distinct phases would have to be present at that composition (Prokhvatilov and Yantsevich 1983; Lunine and Stephenson 1985).

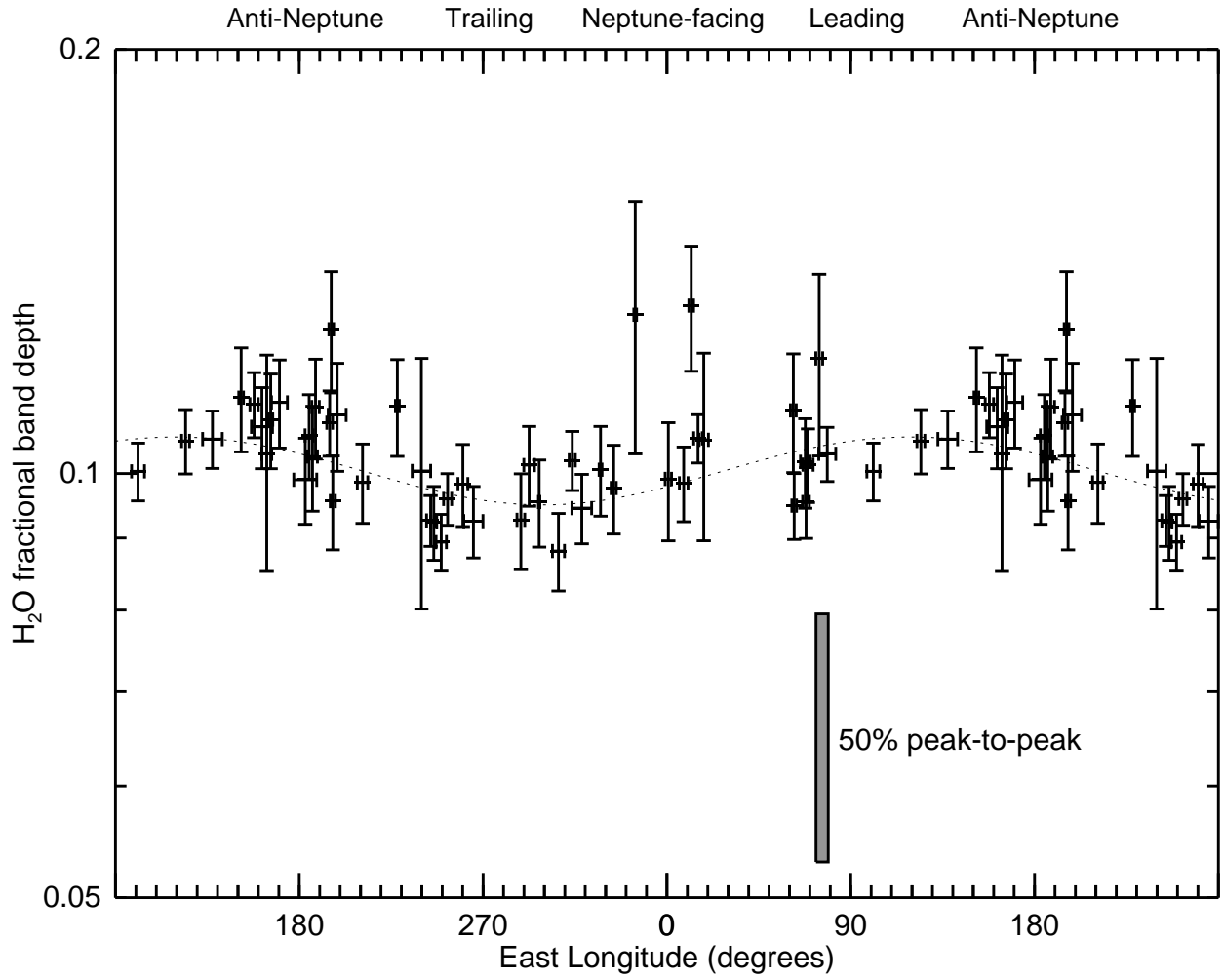


Fig. 6.— Fractional band depth of H<sub>2</sub>O ice as a function of sub-Earth longitude on Triton, showing a subtle enhancement of H<sub>2</sub>O ice absorption on the leading hemisphere ( $12\pm 3\%$  peak-to-peak from the sinusoidal fit shown as a dotted curve).

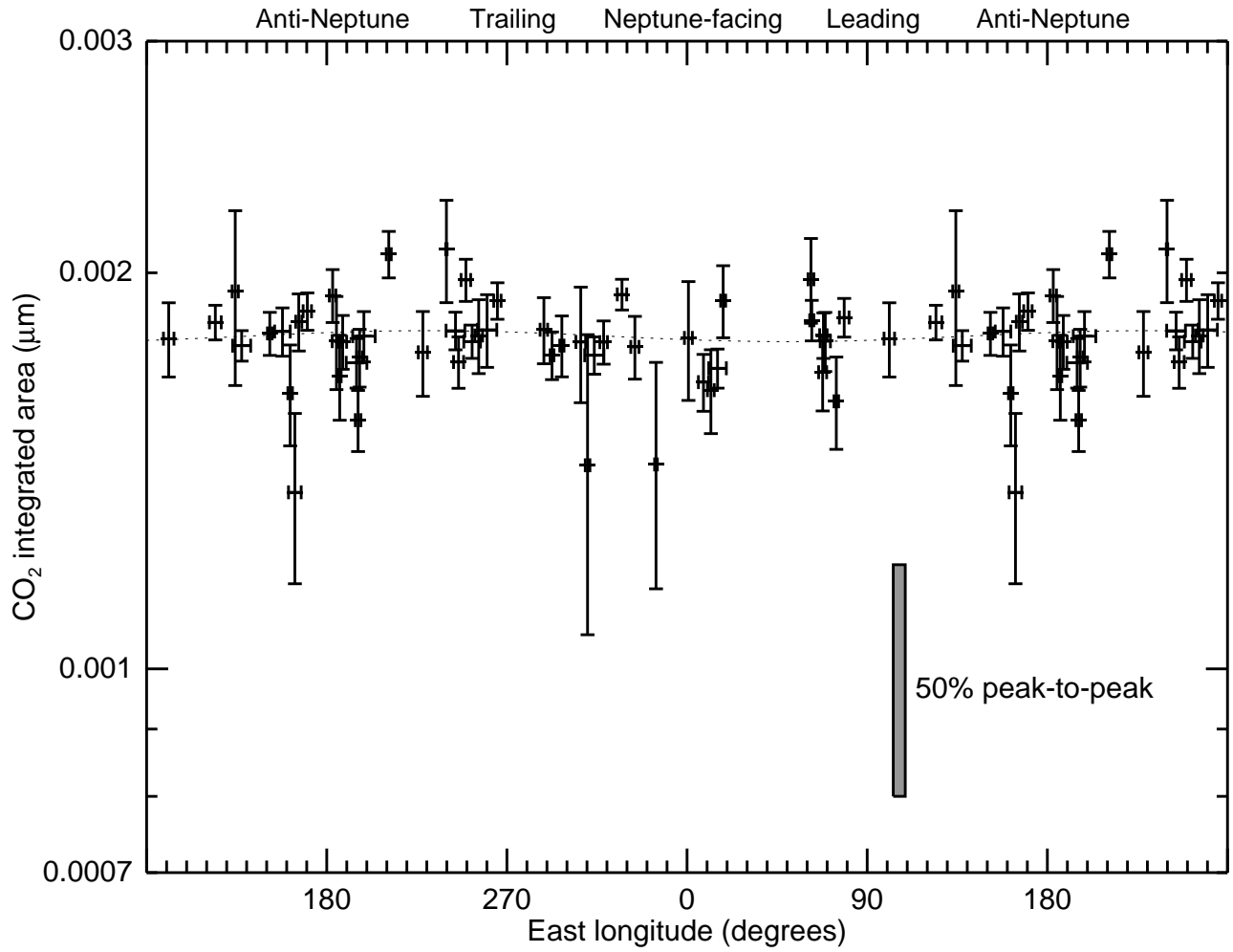


Fig. 7.— Total integrated area of three narrow CO<sub>2</sub> ice absorption bands near 2 μm as a function of sub-Earth longitude on Triton, showing no significant evidence of longitudinal variability ( $2\pm 2\%$  peak-to-peak from the sinusoidal fit shown as a dotted curve).

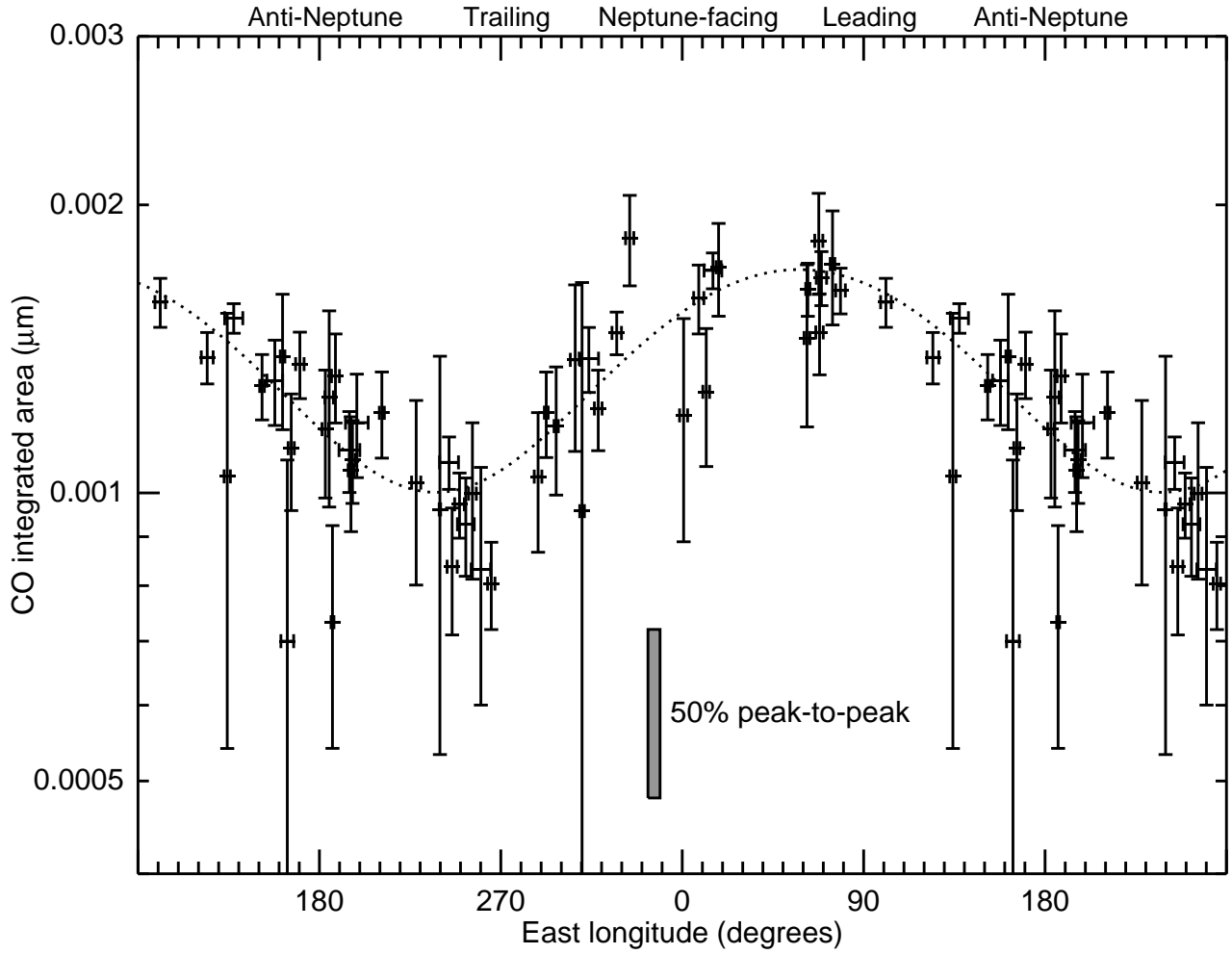


Fig. 8.— Integrated area of the narrow CO ice absorption band at  $2.352 \mu\text{m}$  as a function of sub-Earth longitude on Triton, showing a very similar pattern to that of  $\text{N}_2$  ice.

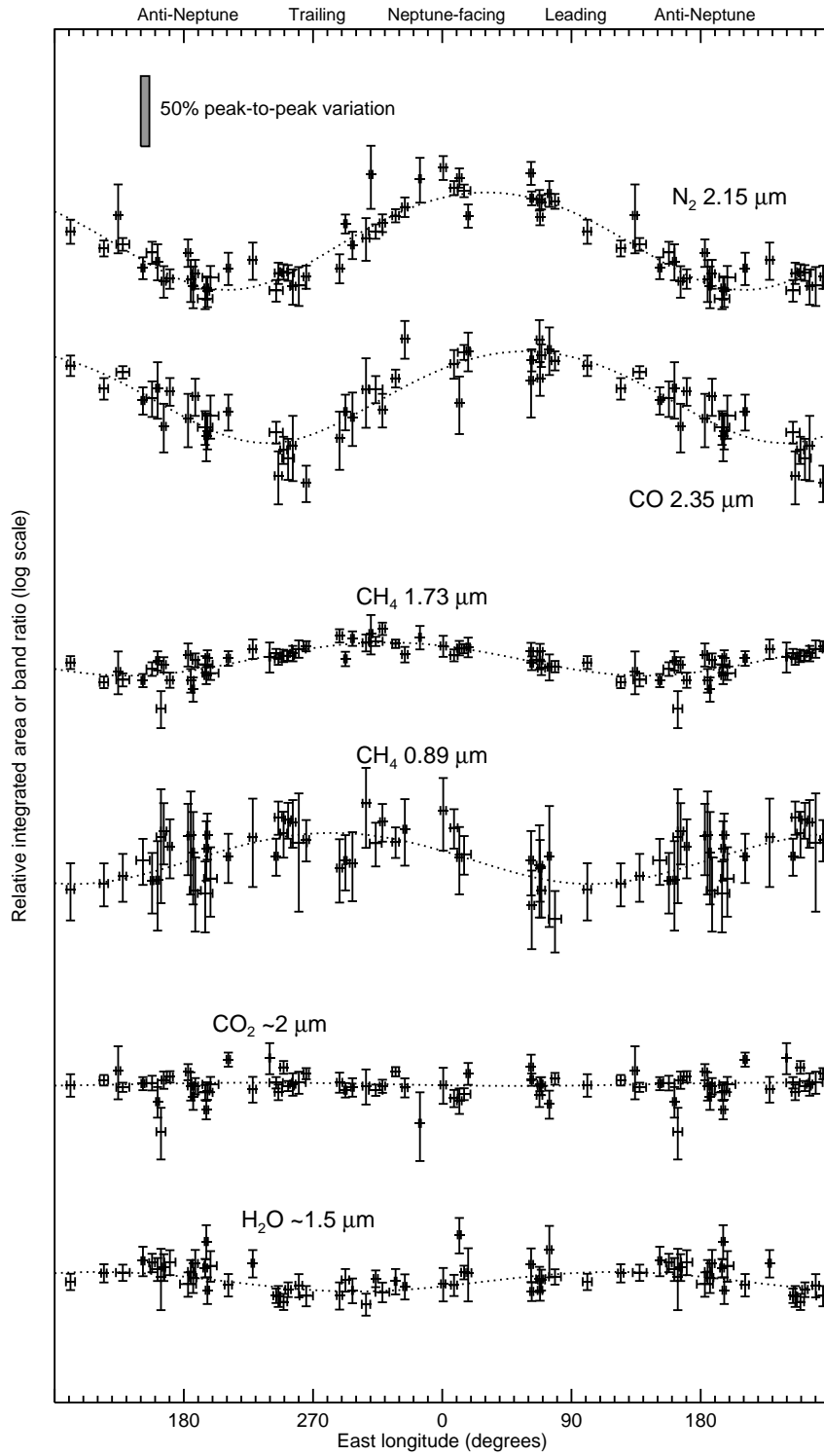


Fig. 9.— Triton’s observed longitudinal spectral variations shown on a consistent logarithmic scale of relative variation.

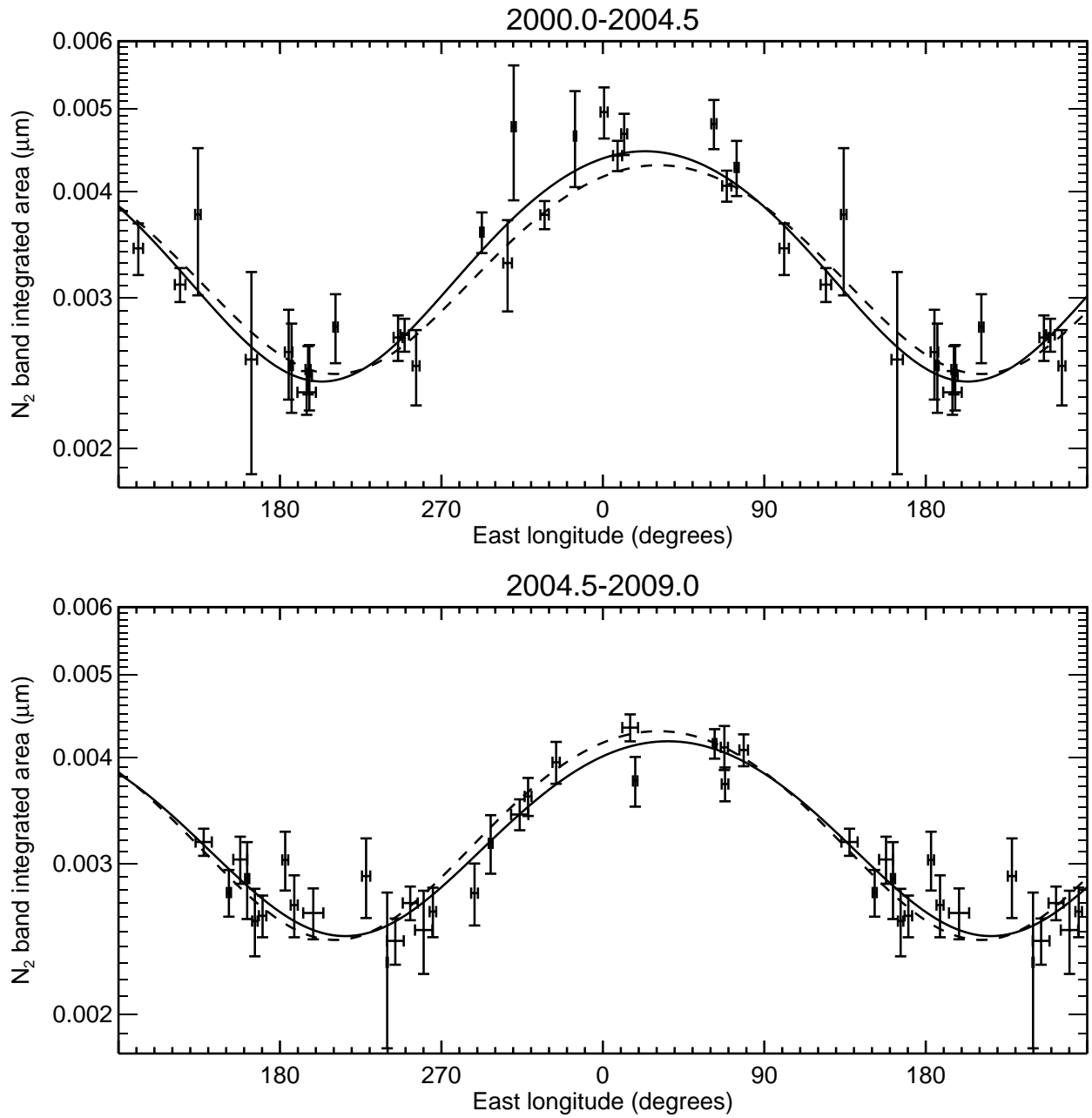


Fig. 10.— Integrated area of the 2.15  $\mu\text{m}$   $\text{N}_2$  ice absorption band split into two 4.5-year time periods. In both panels, the solid curve is a sinusoidal fit to just the data taken during that interval, while the dashed curve is a fit to the full 9-year data set (also shown in Figs. 2 and 9).

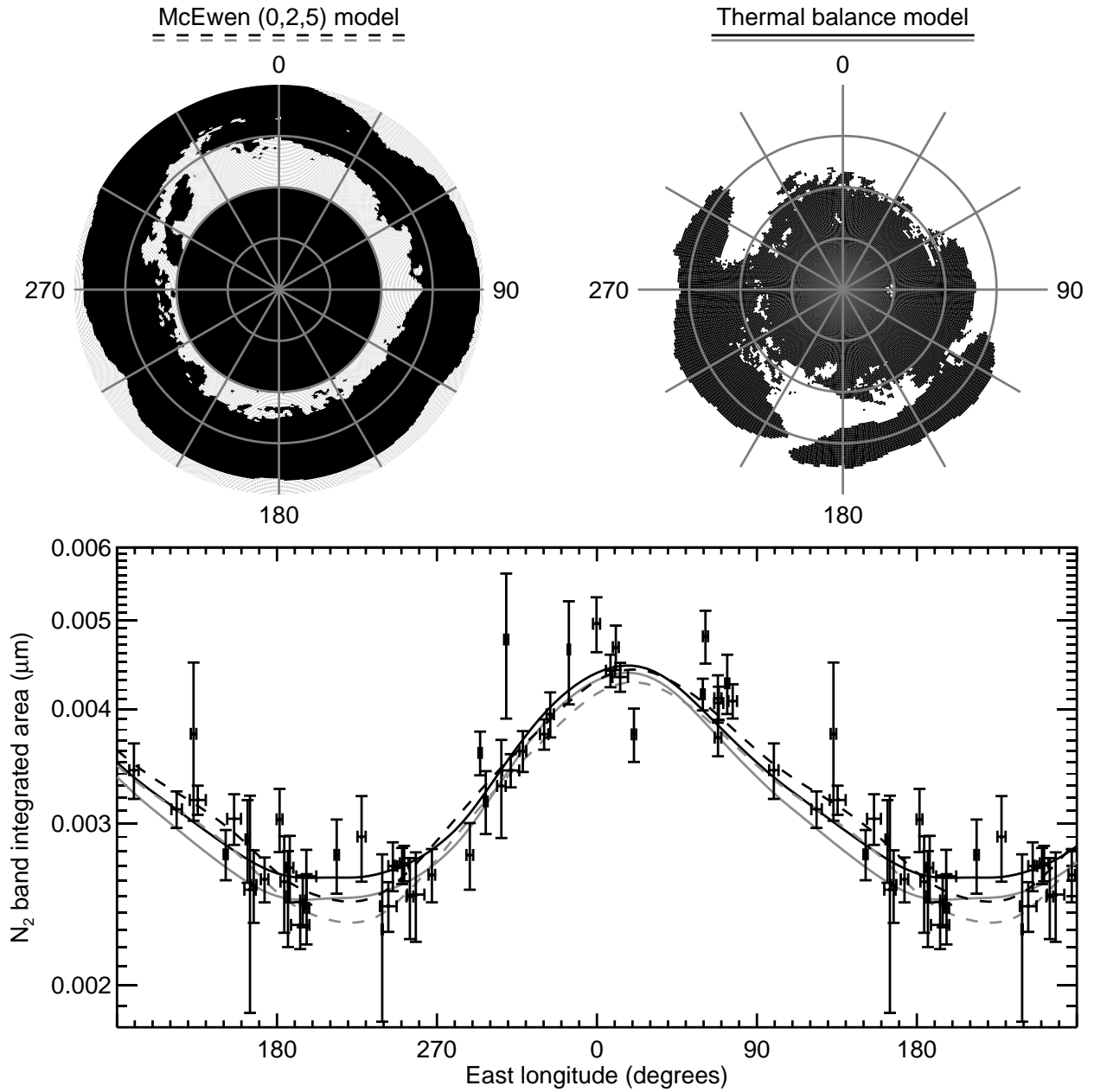


Fig. 11.— Two models for the spatial distribution of Triton’s N<sub>2</sub> ice in South polar projection, with areas free of N<sub>2</sub> ice shown in black and areas covered with N<sub>2</sub> shown in white. Longitude and latitude lines are at 30° intervals. The bottom panel shows the longitudinal variation in the N<sub>2</sub> integrated area, as in Fig. 2. The black curves show the behavior of the McEwen units model (dashed) and the thermal balance model (solid). Gray versions of these curves show how the two models might respond to seasonal recession of N<sub>2</sub> ice coverage.